Gametophytic epigenetic regulators MEA and DME synergistically suppress ectopic shoot formation in *Arabidopsis*

Mohit Rajabhoj[1], Sudev Sankar[1,3], Ramesh Bondada[1,4], Anju P Shanmukhan[2], Kalika Prasad[2]*, Ravi Maruthachalam[1]*

[1]*School of Biology, IISER-Thiruvananthapuram, Thiruvananthapuram, Kerala 695551, India*
[2]*Department of Biology, IISER-Pune, Pune, Maharashtra 411008, India*
[3]Present address: *Department of Plant and Microbial Biology & Zurich-Basel Plant Science Center, University of Zurich, Zollikerstrasse 107, Zurich 8008, Switzerland*
[4]Present address: *Department of Biology and Gus R. Douglass Institute, West Virginia State University, WV 25112-1000, USA*
*Corresponding authors: ravi@iisertvm.ac.in, kalika.prasad@iiserpune.ac.in

Keywords: MEDEA, DEMETER, shoot development, epigenetic regulators, histone methylation, DNA methylation

Running title: MEA and DME control shoot development

Abstract

The gametophyte to sporophyte transition facilitates the alternation of generations in a plant life cycle. The epigenetic regulators DEMETER(DME) and MEDEA(MEA) synergistically control central cell proliferation and differentiation, ensuring proper gametophyte to sporophyte transition in *Arabidopsis*. Mutant alleles of *DME* and *MEA* are female gametophyte lethal, eluding the recovery of recessive homozygotes to examine their role in the sporophyte. Here, we exploited the paternal transmission of these mutant alleles coupled with CENH3-haploid inducer to generate *mea*-1;*dme*-2 sporophytes. Strikingly, the simultaneous loss of function of MEA and DME leads to the emergence of ectopic shoot meristems at the apical pole of the plant body axis. *DME* and *MEA* are expressed in the developing shoot apex and regulate the expression of various shoot-promoting factors. Chromatin immunoprecipitation(ChIP), DNA methylation and gene expression analysis revealed several shoot regulators as potential targets of MEA and DME. Knockdown of upregulated shoot-promoting factors STM, CUC2, and PLT5 rescued the ectopic shoot phenotypes. Our findings reveal a previously unrecognized synergistic role of MEA and DME in restricting the meristematic activity at the shoot apex during sporophytic development to orchestrate the plant architecture.

Introduction

Sporophyte development in higher plants results from a fine balance between cell proliferation and differentiation at the meristems. Primary meristems at the shoot and root apices are responsible for all post-embryonic organ development. This is coordinated by well guided distribution of plant hormones (Stahl and Simon 2010; Ten Hove *et al.* 2015). Throughout this process, epigenetic regulators provide an additional fine-tuning of gene expression, further contributing to plant developmental plasticity. Regulators of Histone methylation like Polycomb Repressive Complex 1 & 2 (PRC1 & PRC2) transcriptionally repress the expression of embryonic genes such as *BABYBOOM* (*BBM*), *LEAFY COTYLEDON1 & 2* (*LEC1* & *LEC2*) to control embryo development (Chen *et al.* 2010). Other epigenetic regulators such as EMBRYONIC FLOWER (EMF)- and VERNALIZATION (VRN)-PRC2s regulate sporophyte development during the transition from the vegetative to the reproductive life phase (Yoshida *et al.* 2001; De Lucia *et al.* 2008). Genes expressed during shoot develop-

ment like *WUSCHEL* (*WUS*), *SHOOT MERISTEMLESS* (*STM*), *AGAMOUS* (*AG*), *BREVIPEDICELLUS* (*BP*), *KNOTTED-LIKE FROM ARABIDOPSIS THALIANA 2* (*KNAT2*), and *KNUCKLES* (*KNU*) are known targets of PRC1 and PRC2 components (Xu and Shen 2008; Chen *et al.* 2016). Their expression pattern is regulated by trimethylation of histone H3 at Lys27 (H3K27me3) repression mark (Kwon *et al.* 2006; Lodha *et al.* 2013; Sun *et al.* 2014; Xiao and Wagner 2015; Xiao *et al.* 2017). Other plants specific transcription factors such as *PLETHORA* (*PLT*) are also epigenetically regulated (Aichinger *et al.* 2011; Lee and Seo 2018). *PLT* genes control both root and shoot development (Prasad *et al.* 2011; Hofhuis *et al.* 2013). *PLT* genes activate the shoot-promoting factor *CUP-SHAPED COTYLEDON2* (*CUC2*) during de novo shoot meristem formation (Kareem *et al.* 2015). CUCs and STM positively regulate each other to maintain stem cell populations and promote organ formation at the shoot apical meristem (SAM) boundary (Spinelli *et al.* 2011). CUCs are also positively regulated by chromatin remodeling factors like BRAHMA (BRM), which is required to establish leaf primordia (Shen and Xu 2009). These studies indicate the maintenance of a delicate balance of CUCs expression during shoot development *via* direct or indirect epigenetic regulators. Apart from controlling shoot development, epigenetic marks such as H3K27me3 and DNA methylation are often reset during major developmental phase transitions, such as gamete and embryo formation (Slotkin *et al.* 2009; Iwasaki and Paszkowski 2014; Borg *et al.* 2020). Such resets facilitate transcription of array of genes in companion cells in gametophyte and floral transition genes in meristem essential to carry out the developmental phase change (Calarco *et al.* 2012; Jullien *et al.* 2012; You *et al.* 2017; Borg *et al.* 2020). Apart from genes, transposable elements (TEs) are also essential for successful developmental phase change (Slotkin *et al.* 2009; Ibarra *et al.* 2012; Higo *et al.* 2020). In absence of DNA methylation and histone modification, TEs express in ectopic tissue and disrupt such phase change events (Lafos *et al.* 2011; Baubec *et al.* 2014).

In *Arabidopsis thaliana*, embryo development is regulated by the components of FERTILIZATION INDEPENDENT SEED-Polycomb Repressive Complex 2 (FIS-PRC2) and DNA glycosylase DEMETER (DME) (Xiao *et al.* 2003; Gehring *et al.* 2006). DME and members of FIS-PRC2 complex like MEDEA (MEA) are primarily expressed in central cells of the embryo sac (Luo *et al.* 2000; Choi *et al.* 2002). The

loss-of-function mutations in these genes result in female gametophyte lethality reflected as parent-of-origin defects during seed development. DME and MEA are known to regulate seed development together, where DME activates the expression of *MEA* in the central cell by removing methylated cytosines (mC's) from *MEA* promoter and intergenic regions (Xiao *et al.* 2003; Gehring *et al.* 2006). DME is expressed in vegetative cell of male gametophyte and it is essential for male gametophyte function (Schoft *et al.* 2011; Park *et al.* 2017, Park *et al*. 2020).

Apart from gametogenesis and seed development, histone methylation mediated by FIS-PRC2 also affects seedling transitions by modulating seed dormancy and repression of embryonic traits in developing seedlings (Bouyer *et al.* 2011). Similarly, DNA methylation is reported to be high in developing seedlings to suppress transposon element expression and maintain an undifferentiated stem cell niche (Bouyer *et al.* 2017; Higo *et al.* 2020). These studies indicate an essential role of DNA and histone methylation in regulating the plant architecture. PRC2 members like MEA and DNA glycosylases like DME are likely to act in transcriptional regulation of target genes. Thus, a complete loss-of-function of *DME* and *MEA* provides an ideal system for examining their function during sporophytic development.

Mutant alleles of *DME* and *MEA* are transmitted through male gamete as microsporogenesis and microgametogenesis remain unaffected in most of these mutants, although *dme* and *mea* are not transmitted through female lineage (Grossniklaus *et al.* 1998; Choi *et al.* 2002; Köhler *et al.* 2003). The generation of homozygous gametophytic lethal mutants thus is challenged by conventional genetic approaches, which rely on self-pollination(inbreeding) of heterozygous single/double mutants to generate respective homozygotes barring those alleles with the leaky transmission. Hence, it is difficult to decipher the role of such gametophyte-lethal genes, if any, in sporophytic development. Studies involving maternal lethals of *DME*, *MEA,* and their epigenetic regulation in sporophytes thus relied either on examining heterozygotes (Roszak and Köhler 2011; Schoft *et al.* 2011; Figueiredo *et al.* 2015; Park *et al.* 2017; Zhang *et al.* 2018; Khouider *et al.* 2021) or homozygous plants carrying a weak allele (Choi *et al.* 2002; Park *et al.* 2017; Simonini *et al.* 2021; Kim *et al.* 2021; Williams *et al.* 2022), thereby restricting complete understanding of their function. Alternative methods to study DME and MEA in sporophyte development have been

employed previously. These include paternal haploids from single mutants, conditional homozygotes, and homozygotic progeny of transheterozygote mutants (Ravi *et al.* 2014; Roy *et al.* 2018; Simonini *et al.* 2021; Kim *et al.* 2021).

Here, we employed haploid genetics to generate viable *mea*$^{-/-}$;*dme*$^{-/-}$ doubled haploid (DH) sporophytes. Using these DH mutant homozygotes, we show that MEA and DME are essential for sporophytic development in *Arabidopsis*. Loss of function of *MEA* and *DME* leads to initiation of ectopic shoot meristems at the apical pole of the plant body axis. We further show that these epigenetic regulators control shoot meristem development by repressing key shoot-promoting factors such as *STM*, *PLT5*, and *CUC2*. Our studies reveal a new role of MEA and DME mediated epigenetic regulation in controlling shoot architecture during post-embryonic development.

Results

mea-1$^{-/-}$;*dme*-2$^{-/-}$ double mutants are viable and initiate functional ectopic SAM

Previous studies have established that MEA and DME play a key role in seed development by regulating polar nuclei and endosperm division after double fertilization (Grossniklaus *et al.* 1998; Choi *et al.* 2002). Several *dme* and *mea* alleles have been isolated by induced mutagenesis from a few select natural *Arabidopsis thaliana* accessions (Choi *et al.* 2002; Guitton *et al.* 2004; Schoft *et al.* 2011). Irrespective of the accession, both *dme* and *mea* mutant alleles can be transmitted through pollen (male) with rare or no maternal female transmission resulting in >25% seed lethality upon self-fertilization of the corresponding heterozygotes. We have earlier shown that generating *mea* and *dme* paternal haploid plants is possible using CENH3-mediated haploid induction (Ravi *et al.* 2014; Roy *et al.* 2018; Supplementary Figure 1). Here, we advanced further to generate doubled haploid (DH) plants of *dme*-2$^{-/-}$ (L*er*), *dme*-6$^{-/-}$, *dme*-7$^{-/-}$(Col-0), and *mea*-1$^{-/-}$ (L*er*), *mea*-6$^{-/-}$, *mea*-7$^{-/-}$ (C24) mutants to examine the recessive vegetative phenotypes associated with *dme* and *mea* mutants (Figure 1A; Supplementary Table 1). Here, we used *dme*-2 and *mea*-1 alleles for generating double homozygotes for the following reasons; firstly, among all the mutant alleles characterized, *mea*-1 and *dme*-2 are reported to show strong loss-of-function phenotypes (Grossniklaus *et al.* 1998; Choi *et al.* 2002; Simonini *et al.* 2021; Kim *et al.* 2021), which is ideal for double mutant studies. Secondly, both alleles are

of the Landsberg *erecta* (L*er*) ecotype, which yields a higher number of spontaneous DH seeds than Columbia (Col-0) (Ravi and Chan 2010). This feature is essential to maximize seed yield to obtain viable spontaneous doubled haploid seeds in the strong gametophyte lethal alleles with high seed abortion like *mea*-1 and *dme*-2. Thirdly, identical L*er* backgrounds of single mutants of *mea* and *dme* ensure genetic homogeneity in the resultant double mutants, thereby avoiding confounding effects due to different genetic backgrounds. We could not generate double mutants of *dme* and *mea* alleles in Col-0 and C24 due to severe seed lethality in these backgrounds (Supplementary Table 1).

mea-1 haploid seedling did not show any visible phenotypic defects and grew normal like wild-type (WT). *mea*-1 haploids yielded spontaneous DH seeds (n=14), of which 2% (n= 21/1178; Supplementary Table 1) were viable, giving rise to *mea*-1$^{-/-}$ DH offspring. Consistent with previous studies, most seeds produced by DH *mea*-1$^{-/-}$ plants were atrophied (81%, n= 1407/1754; Supplementary Figure 1) (Simonini *et al.* 2021). A small fraction of germinated seedlings (4%, n= 14/338) failed to grow two to four days post-germination (dpg). Such seedlings only developed cotyledons and a pair of young leaves. Unlike *mea*-1 haploids, a fraction of *mea*-1$^{-/-}$ (33%, n= 107/324) displayed stunted and aberrant vegetative growth (Supplementary Figure 2). However, when transferred to the soil, these seedlings recovered and showed normal vegetative growth with no discernible phenotypes.

Like *mea*-1 haploids, *dme*-2 haploids also showed normal vegetative growth but severe seed abortion during reproductive development (98%, n= 1286/1308,), owing to the strong loss-of-function of *dme*-2. Spontaneous *dme*-2$^{-/-}$ DH seeds harvested from *dme*-2 haploid plants showed less than 2% germination (n= 22/1308; Supplementary Table 1). About 10% (n= 43/478) of *dme*-2$^{-/-}$ seedlings ceased to grow two to four days post-germination (dpg) (Supplementary Figure 1). Unlike *mea*-1$^{-/-}$ seedlings, a vast majority of *dme*-2$^{-/-}$ seedlings (78%; n= 341/435) exhibited developmental abnormalities such as fused cotyledons, delayed emergence of true leaves, stunted hypocotyl, and retarded root growth (Supplementary Figure 2). Despite these abnormalities, most of the *dme*-2$^{-/-}$ seedlings (n= 153/157) recovered from the early vegetative growth defects when they transitioned to the adult stage, similar to that observed for *mea*-1$^{-/-}$ homozygotes. However, unlike *mea*-1$^{-/-}$ plants, *dme*-2$^{-/-}$ plants

displayed floral defects like altered petal number and positioning, and abnormalities in gynoecium, as reported in earlier studies (Choi *et al.* 2002; Ravi *et al.* 2014; Kim *et al.* 2021; Supplementary Figure 3).

Next, we generated *mea*-1$^{-/-}$;*dme*-2$^{-/-}$ double homozygotes to examine the loss of histone methylation (H3K27me3) and DNA demethylation mediated by MEA and DME, respectively, during early vegetative development of seedlings. To this end, we crossed *mea*-1$^{+/-}$;*dme*-2$^{+/-}$ as a pollen parent, with haploid inducer GFP-*tailswap* as female, and selected *mea*-1;*dme*-2 haploids (n=9/32) and *MEA*;*DME* haploids (n=10/32) by PCR-based genotyping (Figure 1A; Supplementary Figure 1). We collected spontaneous DH seeds from both the haploid sibling genotypes to generate diploid(=DH) *mea*-1$^{-/-}$;*dme*-2$^{-/-}$ and *MEA*$^{+/+}$;*DME*$^{+/+}$ plants. Such *MEA*$^{+/+}$;*DME*$^{+/+}$ DH plants were used as WT control in all our experiments involving *mea*-1$^{-/-}$;*dme*-2$^{-/-}$ mutants.

The DH seeds obtained from *mea*-1;*dme*-2 haploid plants showed less than 1% (n= 13/1950; Supplementary Table 1) viability up to germination (Supplementary Figure 1). The *mea*-1;*dme*-2 haploids showed normal vegetative development like *mea*-1 and *dme*-2 haploids. The selfed *mea*-1$^{-/-}$;*dme*-2$^{-/-}$ plants continued to produce atrophied seeds (n= 1678/1681), as observed in the parent generation. Around 38% (n= 87/226) of germinated *mea*-1$^{-/-}$;*dme*-2$^{-/-}$ were arrested in development and displayed pale and fused cotyledons (Supplementary Figure 2). The remaining viable *mea*-1$^{-/-}$;*dme*-2$^{-/-}$ seedlings displayed severely stunted growth and shorter hypocotyl compared to WT (Figure 1B). Such seedlings also showed underdeveloped and fused cotyledons without petioles compared to WT (Figure 1C-E). We also observed smaller, asymmetric true leaves, indicating defects during shoot development (n= 107/139). Remarkably, nearly half the number of *mea*-1$^{-/-}$;*dme*-2$^{-/-}$ seedlings (n= 71/139) displayed ectopic shoot emerging from the existing shoot apex (Figure 1F, G). Further analysis revealed the initiation of ectopic shoot meristems in *mea*-1$^{-/-}$;*dme*-2$^{-/-}$ (n= 25/48). Figure 1L, M). Like *mea*-1$^{-/-}$ and *dme*-2$^{-/-}$ single mutant plants, *mea*-1$^{-/-}$;*dme*-2$^{-/-}$ plants also recovered from their early developmental defects and displayed normal vegetative growth in the later stages (n= 129/132, Figure 1I; Supplementary Figure 3). In these *mea*-1$^{-/-}$;*dme*-2$^{-/-}$ plants two shoot meristems developed independently and upon transition to reproductive phase, they gave rise to two

inflorescence shoots from a single vegetative body (rosette) (Figure 1I, K; Supplementary Figure 3). This “twin-plant” phenotype is reminiscent of conjoined twins having two independent upper trunks with a common lower portion of the body. The “twin plant” phenotype arising from persistent ectopic shoots suggests a role for DME and MEA in suppressing the initiation of ectopic shoot meristems at apical pole of plant body axis .

Interestingly, a fraction of single mutant *mea*-1 (n= 217/324), *dme*-2 (n= 94/435), and *mea*-1;*dme*-2 double mutants (n=32/139) did not show any visible developmental defects and grew like WT. Even single and double mutant seedlings that show early developmental defects post-germination show resilience at later stages of vegetative development. However, the ectopic shoots initiated during early developmental stages persist throughout the plant life cycle, displaying twin plant phenotype. This observation suggests that the function of both DME and MEA is predominantly required only during juvenile growth but dispensable for later vegetative growth.

MEA and DME are expressed in developing shoot meristems and leaf primordia

Earlier studies have shown that in addition to its gametophyte expression in the central cell of the female gametophyte and in the vegetative cell of the male gametophyte, *DME* is also expressed in sporophytic tissues such as the developing SAMs, root apical meristems (RAMs) and inflorescence meristems (IMs) (Kim *et al.* 2008, Kim *et al.* 2021). Likewise, *MEA* is expressed in the developing embryo till the torpedo stage (Vielle-Calzada *et al.* 1999; Spillane *et al.* 2007) and induced in sporophytic tissues on demand when challenged with pathogens (Roy *et al.* 2018). Further, transcriptome data also indicates the expression of MEA and DME mRNA in the seedlings and other sporophytic tissues (Schmid *et al.* 2005). However, spatiotemporal expression patterns of *MEA* and *DME* in the shoot meristems remained largely unknown. Since we observed ectopic SAM initiation in *mea*-1$^{-/-}$;*dme*-2$^{-/-}$ seedlings, we examined if MEA and DME are expressed in shoot meristem. We first monitored the transcript levels of *MEA* and *DME* in growing seedlings by RT-qPCR. *DME* transcript levels increased in 2 dpg seedlings, with a decline in expression after 3 dpg. Its transcript levels increased after 5 dpg with plant growth (Figure 2A). On the other hand,

we observed *MEA* mRNA expression to be low in the early stage of vegetative development but steadily increased over time till the 10 dpg seedling stage (Figure 2A).

Next, we examined the spatiotemporal expression pattern of DME and MEA using confocal based imaging of the WT plants harboring *pMEA*::*gMEA*:*vYFP* and *pDME*::*gDME*:*vYFP* translational fusions. Both, *pMEA*::*gMEA*:*vYFP* and *pDME*::*gDME*:*vYFP* transgenes were functional and rescued the *mea*-1$^{-/-}$ and *dme*-2$^{-/-}$ mutant phenotypes (Supplementary Figure 4; Supplementary Table 1). The rescue in seed lethality and expression pattern suggests that both the transgenes harbor necessary promoter sequences capable of recapitulating the endogenous expression pattern of *MEA* and *DME*. Consistent with the previous studies, we observed active *MEA* transcription in developing embryos (Vielle-Calzada *et al.* 1999; Spillane *et al.* 2007). We observed *pMEA*::3X-*VENUS* activity during globular stage of embryo. The expression was dispersed and could be detected only in a few cells during later stages of embryo development (n= 33/45) (Figure 2B-F). Unlike *pMEA*::3X-*VENUS*, nearly uniform expression of *pDME*::3X-*VENUS* was observed throughout the embryo development, right from the four celled to the walking-stick stage (n= 66/71) (Figure 2G-K).

Interestingly, during post-embryonic development. *MEA* was predominantly expressed in the peripheral domain of the shoot meristem (Figure 2L). Its expression was also detected in developing leaf primordia (Figure 2N). As reported earlier, *DME* was expressed uniformly throughout the shoot meristem (Figure 2M) (Kim *et al.* 2008, Kim *et al*. 2021). Like *MEA*, its expression was also detected in developing leaf primordia (Figure 2O). Taken together, our studies suggest that the ectopic shoot phenotype in *mea*-1$^{-/-}$;*dme*-2$^{-/-}$ mutant is because of loss of MEA and DME expression in the postembryonic shoot meristems.

MEA and DME repress the expression of shoot-promoting factors

We next examined if the ectopic shoot meristems in *mea*-1$^{-/-}$;*dme*-2$^{-/-}$ made functional stem cell niches. *WUSCHEL* is essential for maintenance of the shoot stem cell niche (Mayer *et al.* 1998; Schoof *et al.* 2000). We therefore monitored the expression of *pWUS*::3X-*VENUS*:*tWUS*, a reporter which specifically marks the shoot stem

cell organizer (Varapparambath *et al.* 2022). Strikingly, *mea*-1$^{-/-}$;*dme*-2$^{-/-}$ seedlings showed ectopic *WUS* promoter activity at the shoot apex (n= 21/48, Figure 3C-D, F, F(i) to F (iii)) as compared to WT seedlings where reporter activity was confined to one organizing center (Figure 3E). Ectopic WUS expression corroborates with shoot phenotype seen in *mea*-1$^{-/-}$;*dme*-2$^{-/-}$. We also observed ectopic WUS-YFP activity in developing cotyledons of *mea*-1$^{-/-}$;*dme*-2$^{-/-}$ embryos and SAM (n= 26/78) indicating aberrant mixed cell fate in the mutant embryo (Figure 3C-D,F). This indicates de novo organizing centers specified in the non-canonical regions in the embryos, as reported earlier (Simonini *et al.* 2021).

We next examined the expression of genes essential for lateral organ initiation. PIN1 expression is an indicator of auxin transport which marks the lateral organ primordia in the developing shoot (Heisler *et al.* 2005). PIN1-GFP was detected in shoot meristem and in developing leaf primordia of ectopic shoots of *mea*-1$^{-/-}$;*dme*-2$^{-/-}$ mutant (n=29/55, Figure 3T). PIN1-GFP expression pattern demonstrates the initiation of leaf primordia in ectopic shoot meristem of the mutant. As expected, PIN1-GFP was expressed in WT and mutant embryos (Figure 3G-R). Similar to WUS, we observed ectopic PIN1 expression in the mutant embryos reinforcing the notion of mixed cell fate identity in the mutant embryos (Figure 3K-R).

We further analyzed the expression of genes that regulate the boundary between the meristem and developing lateral organ primordia. The transcription factor, CUC2, is an early marker of shoot organ boundary specification at SAM (Heisler *et al.* 2005). CUC2 expression in developing embryo displays characteristic stripe formation in the central domain away from protoderm cells till the heart shape stage but later surrounds the SAM between its boundary with cotyledons (Aida *et al.* 1999, 2002) (Figure 3U-X). We monitored CUC2 expression by following *pCUC2*::*CUC2*:*VENUS*; reporter in *mea*-1$^{-/-}$;*dme*-2$^{-/-}$. The typical pattern of CUC2-vYFP in the central domain of embryo was lost. Rather, we observed dispersed expression in SAM initial and protoderm cells (n= 31/77). (Figure 3Y,Z). We observed CUC2-vYFP expression in the cotyledon primordia of a few embryos, further suggesting mixed cell fate identity in the mutant embryos (n=15/77) (Figure 3A’,B’). Interestingly, CUC2-vYFP expression in *mea*-1$^{-/-}$;*dme*-2$^{-/-}$ shoots is dispersed along the peripheral and central zone instead of being restricted at the organ primordia (Figure 3D’). The ectopic expres-

sion of CUC2-vYFP indicates the de-repression of *CUC2* in SAM. These data demonstrate the de-repression of most canonical shoot regulators in *mea*-1$^{-/-}$;*dme*-2$^{-/-}$ seedlings.

Shoot regulators are targets of MEA and DME during early shoot development

The ectopic shoot phenotype in *mea*-1$^{-/-}$;*dme*-2$^{-/-}$ plants and the expression of *DME* and *MEA* in the shoot meristem, prompted us to identify critical targets of MEA and DME that regulate the shoot meristem specification. The interplay between DNA methylation and histone modifications in specifying cell fate and differentiation during development is well-known in animals and plants (Du *et al.* 2015; Williams and Gehring 2020). For instance, a positive feedback loop between DNA methylation and H3K9 methylation maintains the heterochromatin in a repressed state in plants (Du *et al.* 2015). H3K27 methylation, similarly, has been observed predominantly in the heterochromatin state associated with non-CG methylation. The preferential binding of the histone demethylase RELATIVE OF EARLY FLOWERING 6 (REF6) to hypo-methylated DNA leads to the loss of the H3K27me3 mark from the chromatin (Cui *et al.* 2016; Qiu *et al.* 2019). Hence, we hypothesized that a similar interaction between DNA methylation and histone methylation could be jointly mediated by the action of DME and MEA, leading to the regulation of the shoot regulators.

As a histone methyltransferase, MEA catalyzes the trimethylation of H3K27. Hence, to identify targets of MEA, we performed whole genome profiling of H3K27me3 levels by Chromatin Immunoprecipitation (ChIP)-seq experiment. Strikingly, we observed 4993 significant peaks in WT as compared to 4798 peaks in *mea*-1$^{-/-}$;*dme*-2$^{-/-}$ seedlings (Supplementary Table 2). Out of annotated 3885 H3K27me3 binding loci, we selected 431 enriched gene loci for further analysis based on their role in shoot development as predicted by the Gene Ontology Resource (http://geneontology.org/) (Figure 4A; Supplementary Table 2). These 431 genes encompass known shoot regulators like *STM*, *KNAT1*, *CUC2*, *PLT5*, *ESR1 & 2*, *CKX3*, *AHP6*, *KNU*, and *YUC4*. Upon closer examination, we found H3K27me3 binding more persistent in the promoter region (90.4%) of these genes, as reported by earlier studies (Zhang *et al.* 2007; Xiao *et al.* 2016). We also observed differential H3K27me3 binding in the gene body region of *CUC2*, *PLT5*, *STM*, and *WUS* (Figure 4B-E). This loss of in *mea*-1$^{-/-}$;*dme*-2$^{-/-}$ for such genes predicts their active transcription. Indeed, transcript levels of

various shoot regulators which lost the repressive H3K27me3 mark such as STM, CUC2, PLT5, and WUS were increased in the mutant seedlings as compared to WT (Figure 3A-F, U-D', Supplementary Figure 5). Overall, we observed see a de-repression of various shoot regulators, in *mea*-1$^{-/-}$;*dme*-2$^{-/-}$ seedlings.

To examine if loss of function of DME caused any change in methylation landscape of the *mea*-1$^{-/-}$;*dme*-2$^{-/-}$, we performed whole genome bisulfite sequencing on *mea*-1$^{-/-}$;*dme*-2$^{-/-}$ and WT seedlings. We observed a higher CpG and CHG methylation in *mea*-1$^{-/-}$;*dme*-2$^{-/-}$ seedlings (24.60% and 11.10%, Table 1) as compared to WT seedlings (22.50% and 9.80%, Table 1). However, the CHH methylation pattern remained unaffected. This suggests an increase in DNA methylation due to lack of functional DME in the *mea*-1$^{-/-}$;*dme*-2$^{-/-}$ plants. The total number of differentially methylated cytosines (DMCs) are significant (48.54% CpG) in the promoter region (2kb upstream of TSS) of annotated genes of *mea*-1$^{-/-}$;*dme*-2$^{-/-}$ seedlings. However, significant DMCs (more than 25% methylated) were found in the gene body region (72.26% CpG, 44.43% CHG, 65.21% CHH; Figure 4F,G), postulating a transcription activating role of methylation in *mea*-1$^{-/-}$;*dme*-2$^{-/-}$ plants. Gene Ontology analysis of genes associated with such DMCs show numerous genes involved in shoot system development like *A. thaliana RING finger 1A & 1B (AtRING1A & 1B*), *Arabidopsis response regulator 1 & 12* (*ARR1 & ARR12*), RNA-dependent RNA polymerase 6 (*RDR6*) (Figure 4H). For genes like *STM*, *CUC2*, *ESR1*, *ESR2*, *KNAT1 & KNAT6*, we observed subtle hypermethylation in the promoter region (Supplementary Table 3). We also performed CHOP-PCR (Zhang *et al.* 2014; Dasgupta and Chaudhuri 2019) for detecting differentially methylated STM and WUS regulatory regions. We observed weak amplification for *WUS* and *STM* promoter regions in *mea*-1$^{-/-}$;*dme*-2$^{-/-}$ seedlings, indicating methylated DNA region (Supplementary Figure 7). On the other hand, the gene body methylation pattern for such genes showed low levels of hypermethylation at both intronic and exonic cytosines in *mea*-1$^{-/-}$;*dme*-2$^{-/-}$. Although weak, these DNA methylation patterns for *STM*, *CUC2* and *WUS* are suggestive of aiding in the process of transcription, evident with their increase in expression levels in *mea*-1$^{-/-}$;*dme*-2$^{-/-}$ seedlings. DME is also known to positively regulate TEs in developing seeds and pollen grain. Apart from gametophyte, TEs are also differentially expressed in SAM, where they function in regulating genes like *AGO5*,*9* and shoot regulators like *STM*, *CUC2* and *CLV3* (Gutzat *et al.* 2020). We found a significant

number of TEs (6278) to be differentially methylated in *mea*-1$^{-/-}$;*dme*-2$^{-/-}$ seedlings as compared to WT seedlings (Figure 4I). These TEs belong to Gypsy, MuDR, Helitron and COPIA superfamilies (Figure 4I, Supplementary Table 3) known to be specifically expressed in SAM during shoot development (Gutzat *et al.* 2020). Such change in methylation state of these TEs may also be associated with their activation or silencing, as seen during developmental phase change and after treatment with methylation inhibitor (Feng *et al.* 2010; Baubec *et al.* 2014). Here, we report an extension of function of DME in the early sporophytic tissue in regulating TEs expression and their subsequent function of silencing genes important in shoot development.

Table 1. Context-based cytosine methylation associated with genes and transposable elements (TEs). Percent of context-based methylation is calculated using Bismark methylation extraction algorithm.

Context	WT	*mea*-1$^{-/-}$;*dme*-2$^{-/-}$	
		Associated with genes	Associated with TEs
mC's in CpG context, %	15463967, 22.50%	26006159, 24.60%	392421, 6.64%
mC's in CHG context, %	6676430, 9.80%	11864625, 11.10%	465643, 7.88%
mC's in CHH context, %	13466882, 4.40%	22075839, 4.50%	1729891, 29.28%
Total mC's, %	35607279, 36.70%	59946623, 40.20%	2587955, 43.81%

Downregulation of shoot regulators in *mea*-1$^{-/-}$;*dme*-2$^{-/-}$ leads to a partial rescue of the ectopic shoot phenotype

Since the majority of shoot regulators are over-expressed in the SAM of *mea*-1$^{-/-}$;*dme*-2$^{-/-}$ seedlings (Supplementary Figure 5), we sought if down-regulation of some of these shoot regulators viz., STM, PLT5, and CUC2 would suppress the ectopic shoot formation. Our selection of these genes for further analysis is based on their previously implicated role in promoting the shoot meristem formation. For instance, CUC2 and STM were earlier shown to be sufficient for ectopic shoot meristem initia-

tion (Daimon *et al.* 2003; Scofield *et al.* 2008). Furthermore, inducible PLT5 over-expression sufficient for triggering ectopic cell proliferation in the shoot (Supplementary Figure 8).To examine the consequence of down regulating STM, PLT5, and CUC2 in the *mea*-1$^{-/-}$;*dme*-2$^{-/-}$, we performed estradiol-inducible RNAi-mediated gene silencing. Upon estradiol-induced RNAi, *STM mRNA* levels reduced from 5.42-fold to 0.71-fold in *STM-dsRNAi*; *mea*-1$^{-/-}$;*dme*-2$^{-/-}$ seedlings as compared to WT seedlings (Figure 5A). Similarly, *CUC2-dsRNAi* and *PLT5-dsRNAi* decreased *CUC2* and *PLT5 mRNA* levels from 2.52 and 3.54-fold to 0.93 and 0.6-fold, respectively (Figure 5A). Remarkably, ectopic shoot formation was significantly reduced upon reduction of *STM*, or *CUC2*, or *PLT5* transcripts in *mea*-1$^{-/-}$;*dme*-2$^{-/-}$ plants (Figure 5B). Estradiol-induced downregulation of *STM* in *mea*-1$^{-/-}$;*dme*-2$^{-/-}$ germinating seedlings reduced the frequency of ectopic shoot from 49% (N=4, n= 68/139, uninduced mock-treated seedlings; Supplementary Table 1) to 9% (N=4, n= 9/98, estradiol-induced seedlings), suggesting a partial rescue to WT phenotype (N=4, n= 89/98, Figure 5B, C). Similarly, RNAi-mediated knock-down of *CUC2* and *PLT5 mRNA* in *mea*-1$^{-/-}$;*dme*-2$^{-/-}$ germinating seedlings resulted in the reduction of ectopic shoots to 23% (N=3, n= 32/134) and 12% (N=4, n= 28/231), respectively (Figure 5B; Supplementary Figure 9, Supplementary Table 1).

Together, our results suggest that MEA and DME synergistically regulate shoot development by repressing the ectopic induction of shoot-promoting factors.

Discussion

The histone methyltransferase, MEDEA, was identified as imprinted gene with the DNA glycosylase, DEMETER, facilitating its expression in the central cell of the female gametophyte. Both act synergistically to restrict the over-proliferation of the central cell in the absence of double fertilization (Gehring *et al.* 2006). Apart from peculiar seed abortion phenotype, DME was discovered to be aided by H3K27me3 marks on the chromatin, linking it to PRC2 regulated pathway of gene expression (Moreno-Romero *et al.* 2016). Ovules inheriting the strong mutant alleles of both *mea* and *dme* abort seed development, making it impossible to recover homozygotes of either mutant. The maternal lethality of the *mea* and *dme* alleles makes it challenging to examine their roles beyond the gametophyte stage. However, recent studies have successfully implemented various genetic strategies to obtain viable,

single mutant, *mea,* and *dme* homozygotes (Ravi *et al.* 2014; Pires *et al.* 2016; Kim *et al.* 2021; Williams *et al.* 2022). These single mutants have helped demonstrate the role of DME and MEA in various phases of sporophyte development, in addition to its prior established role in the gametophytes. For instance, MEA is required for proper embryonic patterning by regulating cell division via D-type cyclin 1.1 (CYCD1;1) (Simonini *et al.* 2021). MEA also facilitates *P. syringae* infection in *Arabidopsis* by downregulating RESISTANCE TO P. SYRINGAE2 (RPS2) (Roy *et al.* 2018). Like MEA, DME also has a sporophytic role in controlling cell division rate in sporophytic tissues like root hair and stomata, growth of inflorescence stem, and *de novo* shoot regeneration (Kim *et al.* 2021). DME, along with its somatic DNA demethylating counterparts, is also shown to regulate flowering time and inflorescence meristem activity (Kim *et al.* 2021; Williams *et al.* 2022). Like MEA, DME also restricts pathogen infection by repressing transposable elements controlling disease-related proteins in *Arabidopsis* (Schumann *et al.* 2019). In contrast to the documented single mutant phenotypes, *mea*-1$^{-/-}$;*dme*-2$^{-/-}$ plants show a unique presence of twin shoots arising from seed with a single embryo. This suggests the role of MEA and DME in controlling seed to seedling transition phase of sporophytic development.

The rescue of *mea*-1$^{-/-}$;*dme*-2$^{-/-}$ haploid sporophytes using CENH3-mediated genome elimination as a tool facilitated us to generate a population of *mea*-1$^{-/-}$;*dme*-2$^{-/-}$ DH plants which in turn shed light on the synergistic role of MEA and DME in suppressing the activation of ectopic shoot meristems during early sporophyte development. Shoot developmental processes like regeneration and floral transitions are known to be restricted by the repressive histone and DNA methylation marks (Li *et al.* 2011; Sun *et al.* 2014). However, only a few studies have reported the involvement of such epigenetic players during early sporophyte development (Bouyer *et al.* 2011; Gutzat *et al.* 2011). Seed to seedling transition is controlled by FIE, a subunit of the PRC2 complex (Bouyer *et al.* 2011). Here we propose that, during the sporophytic development, MEA, another subunit of the PRC2 complex, and DME restrict the formation of a single meristem at the apical pole by repressing shoot regulators. Consistent with this hypothesis, we show that an array of shoot regulators gets upregulated than WT levels in the *mea*-1$^{-/-}$;*dme*-2$^{-/-}$ mutants.

Restoration of shoot apex typical of wild type by down-regulation of a select few shoot-promoting factors in *mea*-1$^{-/-}$;*dme*-2$^{-/-}$ mutant strengthen this mechanistic framework. Epigenetic suppression of shoot-promoting factors such STM, PLT5, and CUC2 plausibly restrict the coordinated interactions between several fundamental cellular processes such as cell division and differentiation at the apical pole of the plant's body axis during post-embryonic development. It is important to note that MEA and DME do not share common targets. It is likely that MEA and DME mediated distinct regulatory inputs act synergistically to suppress ectopic shoot meristem formation.

In conclusion, we demonstrate an extended synergistic role for the gametophytic epigenetic regulators DME and MEA during the seed-to-seedling transition of sporophyte development. Our study provides the basic framework for understanding the role of gametophytic lethals in sporophytic tissue development. Further studies utilizing haploid induction for generating homozygous mutants may offer more insights into plant growth development.

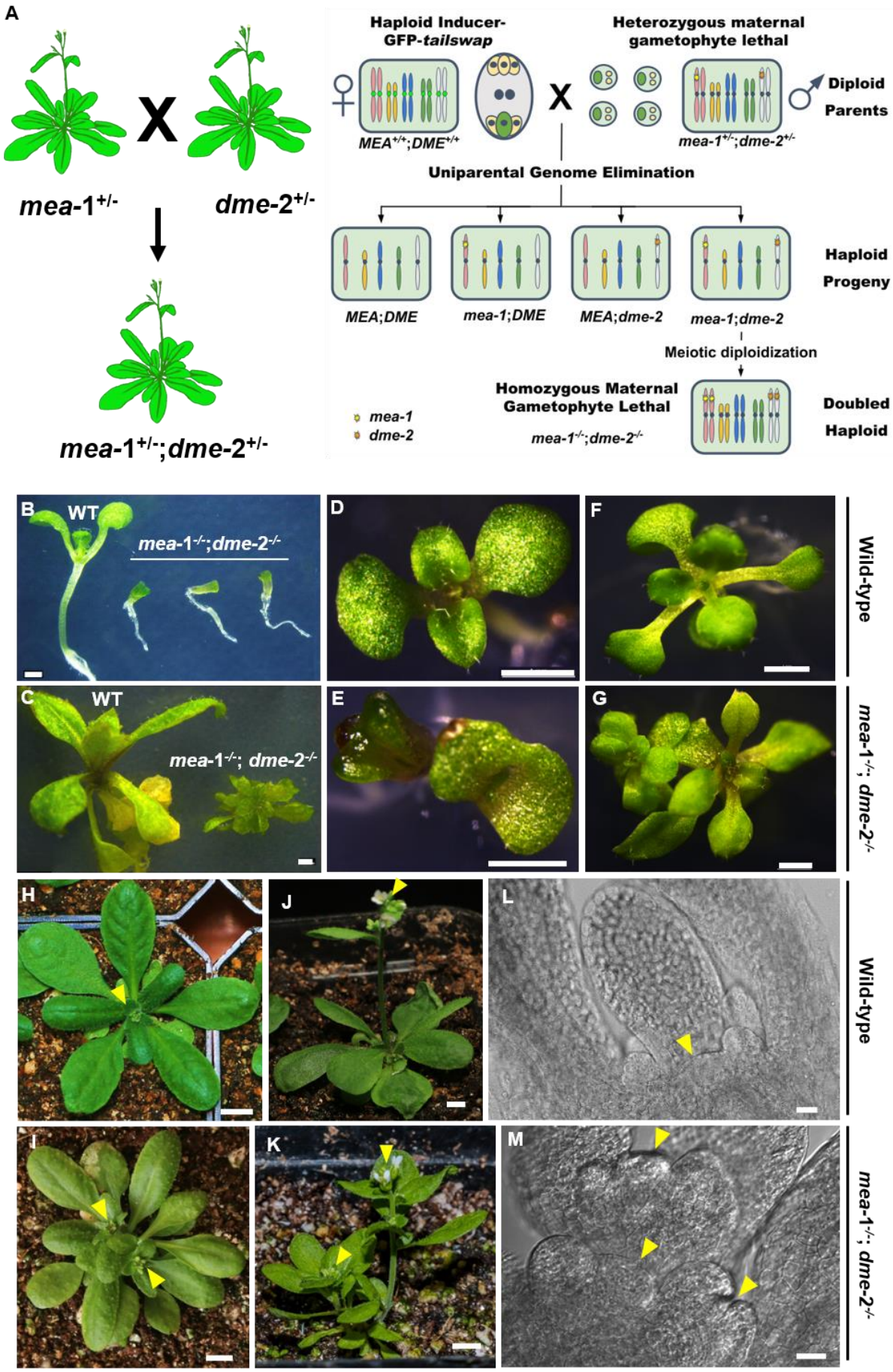
A
mea-1+/-
dme-2+/-
mea-1+/-;dme-2+/-
Haploid Inducer-GFP-tailswap
Heterozygous maternal gametophyte lethal
MEA+/+;DME+/+
mea-1+/-;dme-2+/-
Diploid Parents
Uniparental Genome Elimination
MEA;DME
mea-1;DME
MEA;dme-2
mea-1;dme-2
Haploid Progeny
Meiotic diploidization
Homozygous Maternal Gametophyte Lethal
mea-1
dme-2
mea-1-/-;dme-2-/-
Doubled Haploid
B WT
mea-1-/-;dme-2-/-
C WT
mea-1-/-; dme-2-/-
D
E
F
G
Wild-type
mea-1-/-; dme-2-/-
H
I
J
K
L
M
Wild-type
mea-1-/-; dme-2-/-

468

Figure 1. Generation and phenotypic examination of *mea*-1$^{-/-}$;*dme*-2$^{-/-}$ plants (A) Schematic diagram illustrating rescue of *mea*-1$^{-/-}$;*dme*-2$^{-/-}$ plants using CENH3-mediated genome elimination. **(B,C)** Phenotype of *mea*-1$^{-/-}$;*dme*-2$^{-/-}$ seedlings as compared to WT at 2- leaf (5 dpg) and 6-leaf (10 dpg) stage respectively. Representative images of *MEA*$^{+/+}$;*DME*$^{+/+}$ doubled haploid WT plants at **(D)** 2-leaf (5dpg), **(F)** 6-leaf (10 dpg), **(H)** inflorescence emergence (21 dpg) and **(J)** flowering (28 dpg) stage as compared with *mea*-1$^{-/-}$;*dme*-2$^{-/-}$ plants with ectopic shoot at **(E)** 2-leaf, **(G)** 6-leaf, **(I)** inflorescence emergence and **(K)** flowering stages.

Longitudinal section of shoot apex of the 3-leaf stage (7 dpg) **(L)** WT and **(M)** *mea*-1$^{-/-}$;*dme*-2$^{-/-}$ seedling. Yellow arrowhead is pointing at the shoot apex. Scale bar: **(B-G)**= 1 mm; **(H-K)**= 5 mm; **(L-M)**= 20 µm. dpg: days post germination.

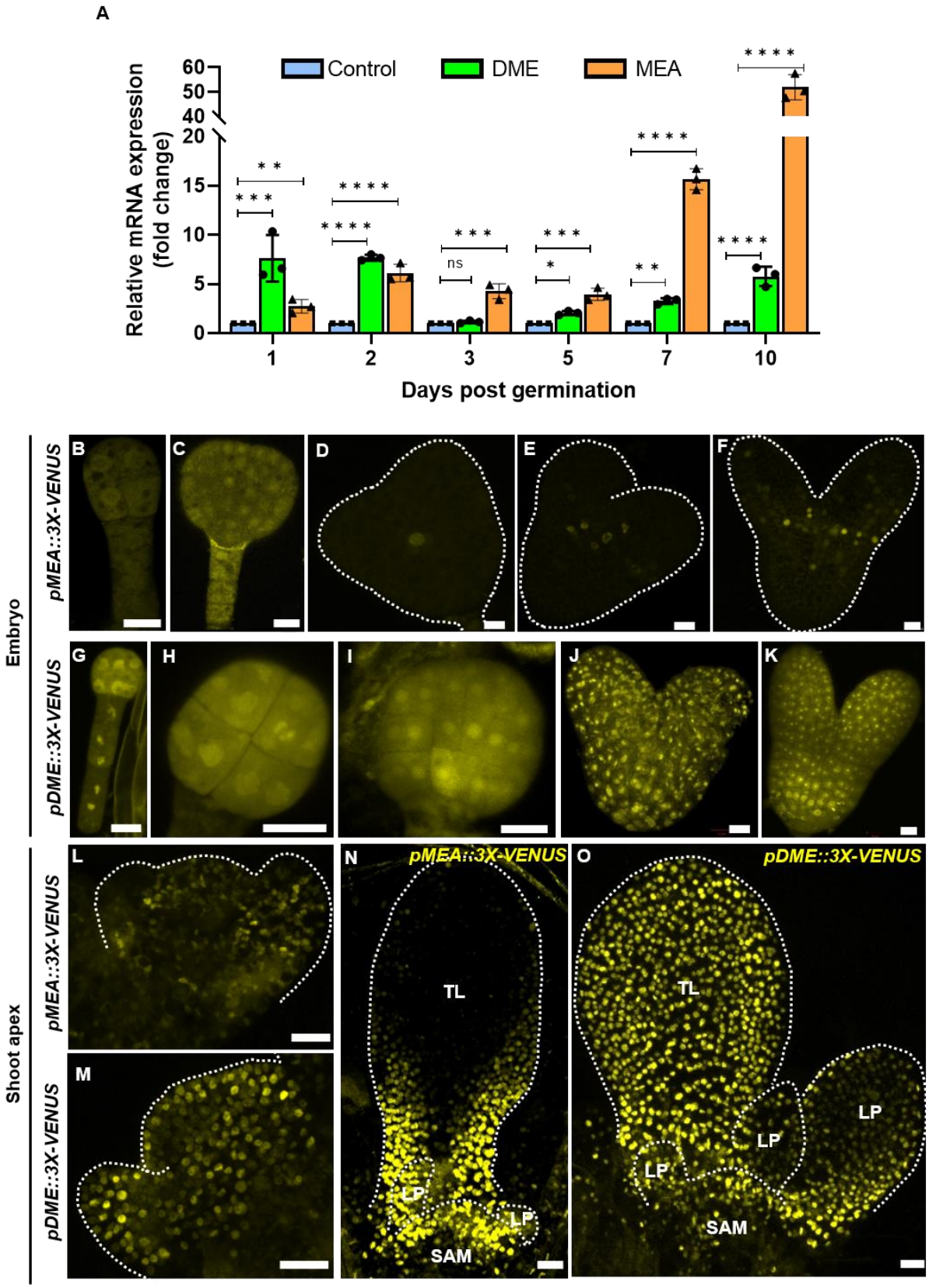
A
Control
DME
MEA
Relative mRNA expression (fold change)
Days post germination
ns
Embryo
pMEA::3X-VENUS
pDME::3X-VENUS
Shoot apex
pMEA::3X-VENUS
pDME::3X-VENUS
TL
LP
SAM

Figure 2. Expression analysis of MEA and DME in sporophytic tissues (A) Relative abundance of MEA and DME mRNA in developing seedlings. *DME* mRNA levels are abundant in 1- and 2-dpg seedlings with sharp decrease in its level on 3- and 5-dpg (1-dpg: 7.62±2.37, ***p*= 0.0016; 2-dpg: 7.69±0.30, *****p*= 0.000003; 3-dpg: 1.15±0.13, ^{ns}p= 0.11; 5-dpg: 2.06±0.20, ***p*= 0.003; 7-dpg: 3.28±0.29, ****p*=0.00084; 10-dpg: 5.79±0.99, ***p*= 0.0033). *MEA* mRNA levels gradually increased as the seedling transitioned from 1- to 10-dpg (1-dpg: 2.76±0.69, **p*= 0.011; 2-dpg: 6.12±0.89, ***p*= 0.0023; 3-dpg: 4.27±0.76, ***p*= 0.0034; 5-dpg: 3.97±0.62, ***p*= 0.0033; 7-dpg: 15.66±1.08, *****p*=0.0001; 10-dpg: 51.96±5.12, ****p*= 0.00033). Statistical test: Multiple unpaired *t*-tests (Holm-Sidak method), with alpha = 0.05. Error bar: SD.

(B-O) Representative images of embryos and shoot apices showing expression patterns of **(B-F, L,N)** *pMEA*::3X- *VENUS* and **(G-K, M,O)** *pDME*::3X-*VENUS.*

pMEA::3X-*VENUS* expression (yellow) in developing embryo **(B)** octant, **(C)** globular, **(D)** early heart-shape, **(E,F)** heart-shape **(L)** SAM and in **(N)** shoot apex.

pDME::3X-*VENUS* expression (yellow) in developing embryo **(G)** octant, **(H)** dermatogen **(I)** globular, **(J)** heart-shape **(K)** late heart-shape **(M)** SAM and **(O)** shoot apex. SAM- shoot apical meristem, LP-leaf primordium, TL- true leaf. Scale bar: **(B-K)**= 10 µm; **(L-O)**= 20 µm.

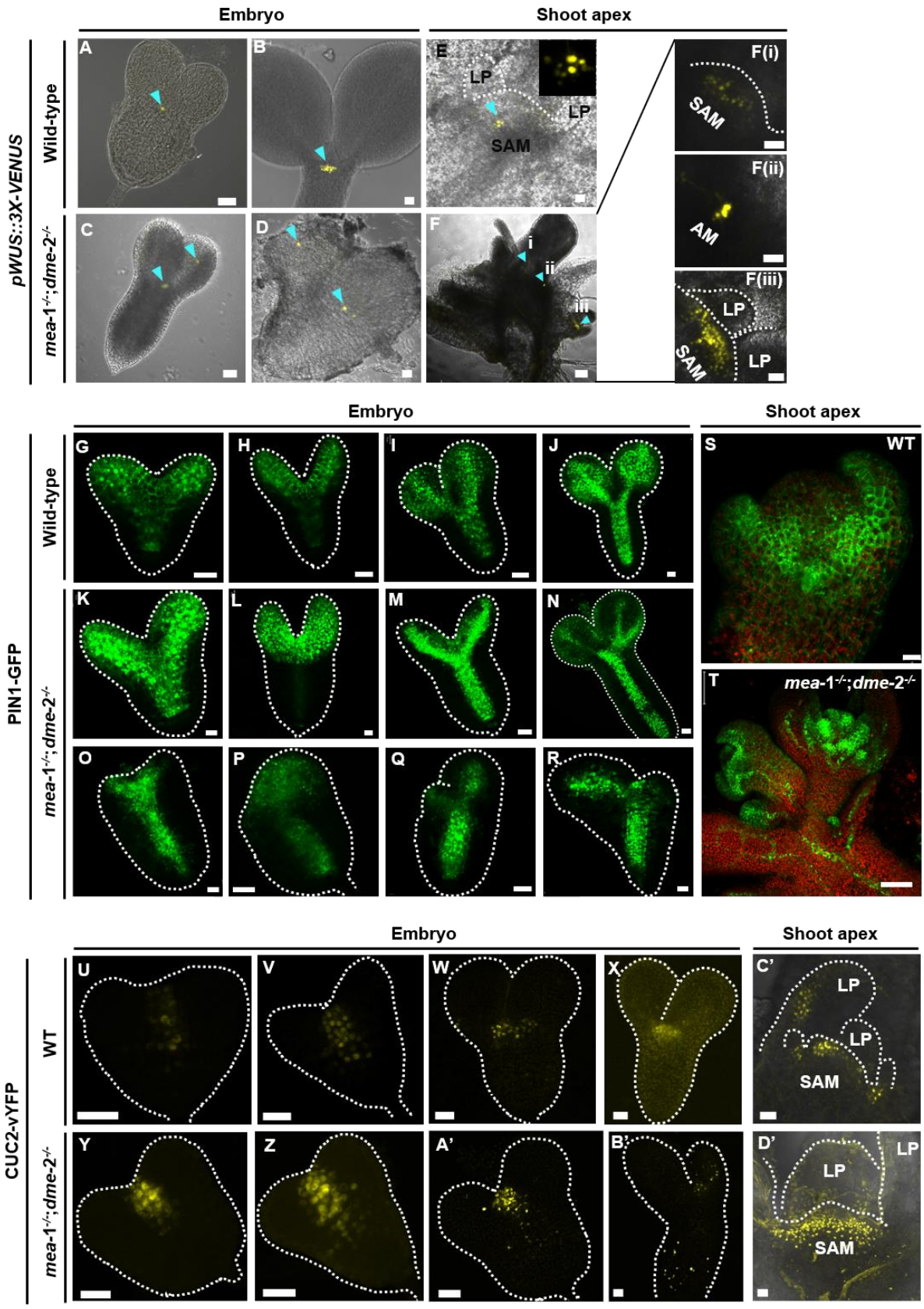
Embryo
Shoot apex
pWUS::3X-VENUS
Wild-type
mea-1-/-;dme-2-/-
A
B
C
D
E
F
LP
SAM
i
ii
iii
F(i)
F(ii)
F(iii)
AM
PIN1-GFP
G
H
I
J
K
L
M
N
O
P
Q
R
S
WT
T
mea-1-/-;dme-2-/-
CUC2-vYFP
U
V
W
X
Y
Z
A'
B'
C'
D'

501

502

Figure 3. Deregulated expression pattern of shoot regulators in *mea*-1$^{-/-}$;*dme*-2$^{-/-}$ embryos and seedling (A-D') Representative images of embryos and shoot apices showing expression pattern of **(A-F(iii))** *pWUS*::3X-*VENUS,* **(G-T)** PIN1-GFP and **(U-D')** CUC2-vYFP shoot regulators.

pWUS::3X-*VENUS* expression (yellow) in organizing center of embryos of **(A-B)** wild-type and **(C-D)** *mea*-1$^{-/-}$;*dme*-2$^{-/-}$ *(*n= 26/78) showing ectopic organizing center in cotyledon (marked with yellow arrowhead). *WUS*::3X-VENUS is marking center of shoot meristem in **(E)** wild-type, inset is showing organizing center in SAM and **(F to F(iii))** *mea*-1$^{-/-}$;*dme*-2$^{-/-}$,along with **(F(i))** primary shoot meristem **(F(ii))** axillary meristem and **(F(iii))** ectopic shoot meristem, marked with blue arrowhead (n=21/48). The meristem dome (SAM) and leaf primordia (LP) are labeled and indicated with a white dashed line. The scale bar represents 20 µm in **(A-E)** and **(F(i) to F(iii))**, and 100 µm in **(F)**.

PIN1-GFP (green) expression in embryos of **(G-J)** wild-type and **(K-R)** *mea*-1$^{-/-}$;*dme*-2$^{-/-}$ showing ectopic PIN1 expression. Dashed lines outline the embryo shape. PIN1-GFP expression in shoot meristem of **(S)** wild-type **(T)** *mea*-1$^{-/-}$;*dme*-2$^{-/-}$ seedling showed PIN1 expression in ectopic shoot along with primary shoot (n=29/55) along with red as autofluorescence. The scale bar represents 20 µm in **(G-R)** and100 µm in **(S-T)**.

CUC2-vYFP (yellow) expression in embryos of **(U-X)** wild-type and **(Y-B')** *mea*-1$^{-/-}$;*dme*-2$^{-/-}$ showing ectopic expression at SAM and developing cotyledons (n= 31/77). CUC2-vYFP expression in shoot apex of **(C')** wild-type and **(D')** *mea*-1$^{-/-}$;*dme*-2$^{-/-}$ showing ectopic expression in SAM apart from leaf primordia (n= 15/77). The scale bar represents 20 µm. SAM- shoot apical meristem, AM- axillary meristem, LP-leaf primordium.

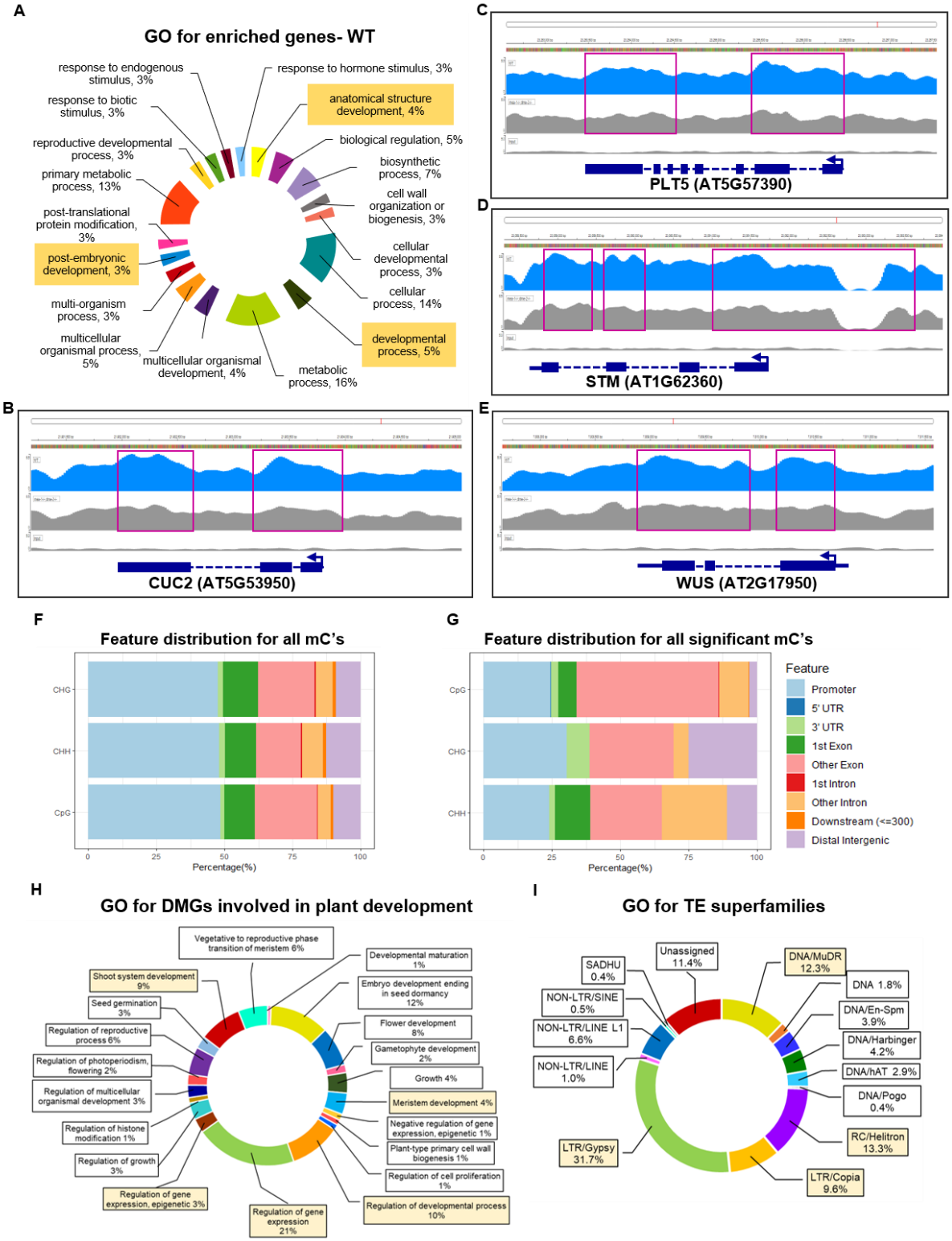
A
GO for enriched genes- WT
response to endogenous stimulus, 3%
response to hormone stimulus, 3%
response to biotic stimulus, 3%
anatomical structure development, 4%
reproductive developmental process, 3%
biological regulation, 5%
primary metabolic process, 13%
biosynthetic process, 7%
post-translational protein modification, 3%
cell wall organization or biogenesis, 3%
post-embryonic development, 3%
cellular developmental process, 3%
cellular process, 14%
multi-organism process, 3%
developmental process, 5%
multicellular organismal process, 5%
multicellular organismal development, 4%
metabolic process, 16%
C
PLT5 (AT5G57390)
D
STM (AT1G62360)
B
CUC2 (AT5G53950)
E
WUS (AT2G17950)
F
Feature distribution for all mC's
CHG
CHH
CpG
0
25
50
75
100
Percentage(%)
G
Feature distribution for all significant mC's
CpG
CHG
CHH
Feature
Promoter
5' UTR
3' UTR
1st Exon
Other Exon
1st Intron
Other Intron
Downstream (<=300)
Distal Intergenic
H
GO for DMGs involved in plant development
Vegetative to reproductive phase transition of meristem 6%
Developmental maturation 1%
Shoot system development 9%
Embryo development ending in seed dormancy 12%
Seed germination 3%
Flower development 8%
Regulation of reproductive process 6%
Gametophyte development 2%
Regulation of photoperiodism, flowering 2%
Growth 4%
Regulation of multicellular organismal development 3%
Meristem development 4%
Negative regulation of gene expression, epigenetic 1%
Regulation of histone modification 1%
Plant-type primary cell wall biogenesis 1%
Regulation of growth 3%
Regulation of cell proliferation 1%
Regulation of gene expression, epigenetic 3%
Regulation of developmental process 10%
Regulation of gene expression 21%
I
GO for TE superfamilies
Unassigned 11.4%
SADHU 0.4%
DNA/MuDR 12.3%
NON-LTR/SINE 0.5%
DNA 1.8%
NON-LTR/LINE L1 6.6%
DNA/En-Spm 3.9%
DNA/Harbinger 4.2%
NON-LTR/LINE 1.0%
DNA/hAT 2.9%
DNA/Pogo 0.4%
RC/Helitron 13.3%
LTR/Gypsy 31.7%
LTR/Copia 9.6%

Figure 4. Validation of targets of MEA and DME (A) Gene ontology (GO) of enriched genes in ChIP using αH3K27me3. **(B-E)** Graphical representation of ChIP-seq using αH3K27me3 for **(B)** *STM*, **(C)** *CUC2* **(D)** *PLT5* and **(E)** *WUS* gene and their upstream region. Pink boxes denote prominent enrichment in WT ChIP DNA as compared to *mea*-1$^{-/-}$;*dme*-2$^{-/-}$ ChIP DNA. Input DNA is WT DNA without αH3K27me3 treatment. **(F-G)** Distribution of methylation locations at **(F)** across the genome and **(G)** at significant (≥25% methylation, $q<0.01$, $p>0.05$) locations. **(H-I)** GO analysis for differentially methylated **(H)** genes (DMGs) involved in plant development **(I)** Transposable elements (TEs) classified in superfamilies.

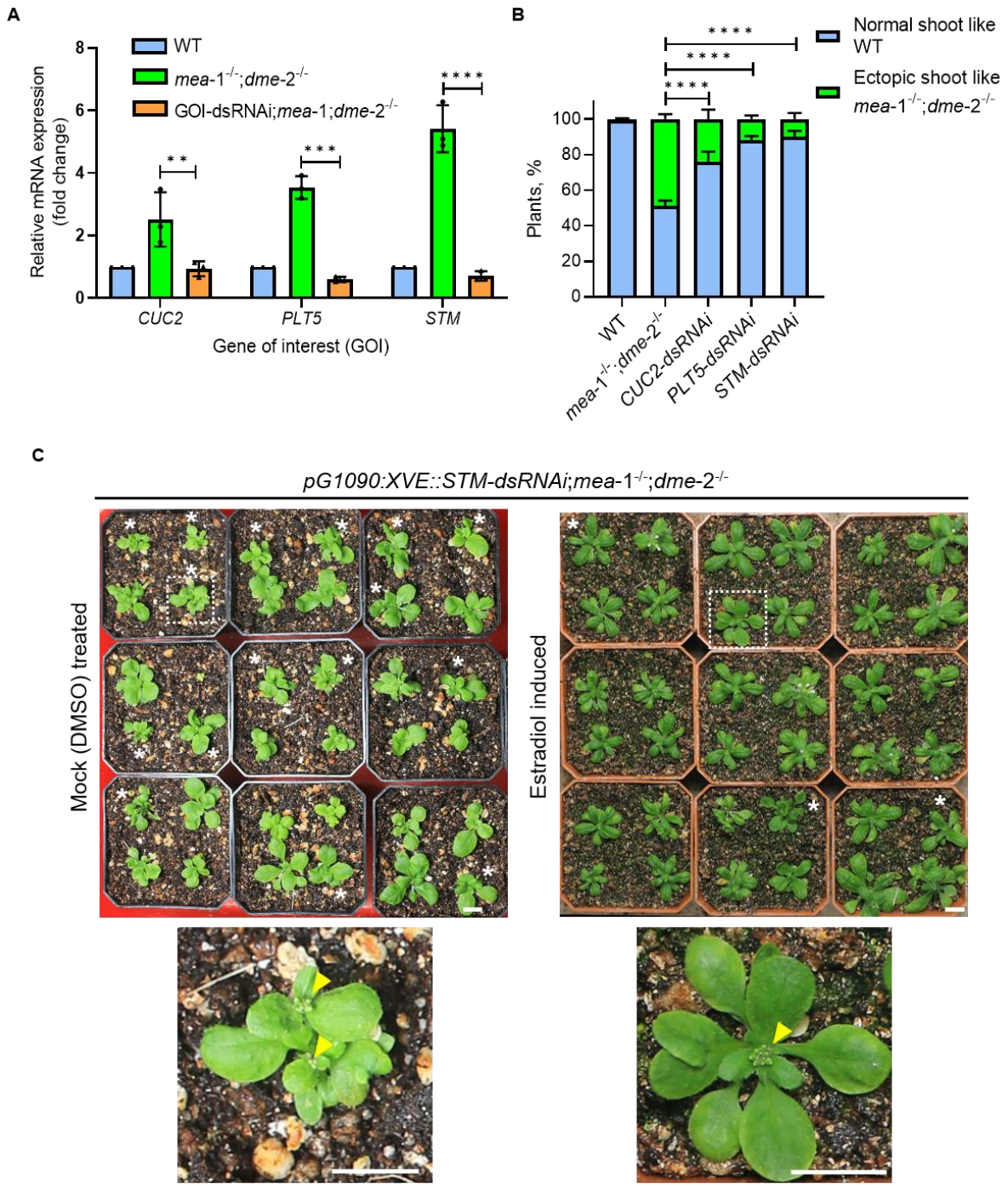
A
WT
mea-1-/-;dme-2-/-
GOI-dsRNAi;mea-1;dme-2-/-
Relative mRNA expression (fold change)
CUC2
PLT5
STM
Gene of interest (GOI)
B
Normal shoot like WT
Ectopic shoot like mea-1-/-;dme-2-/-
Plants, %
WT
mea-1-/-;dme-2-/-
CUC2-dsRNAi
PLT5-dsRNAi
STM-dsRNAi
C
pG1090:XVE::STM-dsRNAi;mea-1-/-;dme-2-/-
Mock (DMSO) treated
Estradiol induced

Figure 5. RNAi mediated downregulation of select target genes. (A) Relative abundance of *CUC2*, *PLT5*, and *STM* transcripts in respective RNAi lines. *CUC2*: WT- 1±0, *mea*-1$^{-/-}$;*dme*-2$^{-/-}$- 2.52±0.87, *CUC2*-dsRNAi;*mea*-1$^{-/-}$;*dme*-2$^{-/-}$- 0.94±0.24, **p*=0.038; *PLT5*: WT- 1±0, *mea*-1$^{-/-}$;*dme*-2$^{-/-}$- 3.54±0.36, *PLT5*-dsRNAi;*mea*-1$^{-/-}$;*dme*-2$^{-/-}$- 0.60±0.08, ****p*=0.00048; *STM*: WT- 1±0, *mea*-1$^{-/-}$;*dme*-2 $^{-/-}$- 5.42±0.75, *STM*-dsRNAi;*mea*-1$^{-/-}$;*dme*-2$^{-/-}$- 0.71±0.15, ****p*=0.0008. Statistical test: Multiple unpaired *t*-tests (Holm-Sidak method), with alpha = 0.05. Error bar: SD.

(B) Quantification of shoot number in *CUC2*-, *PLT5*- and *STM*-RNAi lines as compared to WT and *mea*-1$^{-/-}$;*dme*-2$^{-/-}$. WT: n= 161 (Normal shoot= 161, ectopic shoot= 0); *mea*-1$^{-/-}$;*dme*-2$^{-/-}$: n= 139 (Normal shoot= 71, ectopic shoot= 68); *CUC2*-dsRNAi;*mea*-1$^{-/-}$;*dme*-2$^{-/-}$: n= 134 (Normal shoot= 102, ectopic shoot= 32, *****p*< 0.0001); *PLT5*-dsRNAi;*mea*-1$^{-/-}$;*dme*-2$^{-/-}$: n= 231 (Normal shoot= 203, ectopic shoot= 32, *****p*< 0.0001); *STM*-dsRNAi;*mea*-1$^{-/-}$;*dme*-2$^{-/-}$: n= 98 (Normal shoot= 89, ectopic shoot= 9, *****p*< 0.0001). Statistical analysis: two-way ANOVA (Sidak method), with alpha = 0.05. Error bar: SEM.

(C) Rescue of ectopic shoot in estradiol-induced *STM*-dsRNAi;*mea*-1$^{-/-}$;*dme*-2$^{-/-}$ plants. Asterix(*) marks plants with ectopic shoots. White dotted box corresponds to the zoomed plants shown in the below panel. Yellow arrowhead points to the shoot apex. Scale bar: 1cm.

Materials and Methods

Plant materials and growth conditions

Arabidopsis thaliana seeds were surface sterilized by fumigation with Chlorine (Cl_2) gas (Lindsey *et al.* 2017). Fumigated seeds were then plated onto Murashige and Skoog (MS) growth medium with 0.8% agar and cold stratified at 4℃ in dark for four days. After cold stratification, the plates were transferred to the growth chamber for germination. Seedlings and plants in pots were grown under white fluorescent lights (7000 lux at 20 cm) at 22 °C with a 16 h light/8 h dark cycle at 75% RH in a controlled growth cabinet (Percival Inc.). Heterozygous *MEA*/*mea*-1 (Grossniklaus *et al.* 1998) and *DME*/*dme*-2 (Choi *et al.* 2002) mutants were previously described. Following heterozygous seeds were obtained from Arabidopsis Biological Resource Center: *MEA*/*mea*-6 (CS6996), *MEA*/*mea*-7 (CS6997), *DME*/*dme*-6 (GK-252E03), and *DME*/*dme*-7 (SALK107538).

Generation of maternal gametophytic lethal homozygotes

To generate *dme*-2 (AT5G04560) and *mea*-1 (AT1G02580) homozygous mutants, heterozygous *DME*/*dme*-2 and *MEA*/*mea*-1 plants were crossed as the male to haploid inducer GFP-*tailswap* plants as female (Ravi *et al.* 2014). The resultant F1 seeds were collected and germinated on Murashige and Skoog agar plates and later transferred to soil for further growth. Haploids were identified phenotypically and cytologically as described earlier (Ravi and Bondada 2016). All the haploids were PCR genotyped to identify the *DME* WT allele using MR146 and MR147 oligo combinations amplifying a 791 bp fragment. Similarly, the *dme*-2 mutant haploids were identified using MR147 and a left border-specific oligo MR148 producing 381 bp fragment. *MEA* allele was identified using oligonucleotides combinations MR8 and MR319 (722 bp), and the *mea*-1 allele using MR8 and a left border-specific oligo MR10 (312 bp). The DNA sequences for all oligos used in this study is given in Supplementary Table 5. The mutant haploids were screened for spontaneous mitotic/meiotic doubling events for obtaining doubled haploid seeds which gives rise to homozygous mutant diploid sporophytes. For generating homozygous *mea*-1;*dme*-2 double mutant in L*er* ecotype, *mea*-1 homozygous plants serving as female parent were crossed with *dme*-2 heterozygous plants as male parent. The resulting progeny PCR genotyped

for both the *mea*-1 and *dme*-2 alleles, and the plants heterozygous plant both *mea*-1 and *dme*-2 alleles were identified and used as male parent in a cross with GFP-*tailswap* as female. *mea*-1;*dme*-2 haploid plants were identified using PCR-based genotyping. Spontaneous double haploid seeds from *mea*-1;*dme*-2 plants were collected to generate *mea*-1;*dme*-2 doubled haploid (diploid) sporophytes used in this study.

Quantitative Real Time-PCR

For expression analysis of *DME* and *MEA* mRNA, we harvested shoot apices from 1, 3, 5, 7, and 10 dpg old WT seedlings and stored at -80℃ for further use. Shoot apices from *mea*-1$^{-/-}$;*dme*-2$^{-/-}$ seedlings were used as control. Total RNA was isolated using TRIzol™ reagent as per the manufacturer's instructions. The extracted RNA was treated with NEB(New England Biolabs) DNase I (RNase free) (M0303) according to NEB guidelines to remove the genomic DNA contamination. One microgram of total RNA was used for complementary DNA (cDNA) synthesis by PrimeScript first strand cDNA synthesis kit (TAKARA-Bio, Cat# 6110) using an oligo(dT) and random hexamer as oligonucleotides. qPCRs were performed on Mastercycler BIORAD CFX96™ using the oligonucleotides mentioned in Supplementary Table 5. *ACTIN2* (*ACT2*) served as a reference gene control. The reactions were carried out using TB Green® Premix Ex Taq™ II (TAKARA-Bio, Cat no. RR82WR) and incubated at 95 °C for 2 minutes, followed by 40 cycles of 95 °C for 15 s and 60 °C for 30 s. PCR specificity was checked by melting curve analysis. *ACT2* was used for the normalization for all the reactions. At least three independent biological samples were analyzed for each time point mentioned above, and qPCR reactions were set up with three technical replicates for each biological replica. mRNA abundance of target genes was analyzed (Supplementary Table 4) using the normalized $2^{-\Delta\Delta Ct}$ (cycle threshold) method (Livak and Schmittgen 2001).

ChIP followed by Next-Generation Sequencing

To identify the targets of MEA protein and differentiate histone methylation, we performed chromatin immunoprecipitation (ChIP) followed by next-generation sequencing as described previously (Yamaguchi *et al.* 2014; Salvi *et al.* 2020) on two independent biological replicates. 500 mg of micro dissected shoot apices, devoid of cot-

yledons and hypocotyl, from 2 to 3-day-old WT and *mea*-1$^{-/-}$;*dme*-2$^{-/-}$ seedlings were used for each sample. The samples were fixed in 1.8% formaldehyde in 1X PBS and vacuum infiltrated for 15 mins at room temperature to cross-link the tissue. After fixation, formaldehyde solution was removed and replaced by ice-cold 0.125 M glycine solution (in 1X PBS) followed by vacuum infiltration for 5 mins to quench the reaction. The glycine solution was filtered away and samples were washed twice with ice-cold 1X PBS. Samples were blotted on Kim wipe paper to remove excess 1X PBS. Samples were frozen and powdered in liquid nitrogen. The powdered samples were resuspended in nuclei extraction buffer (50 mM Tris-HCl pH 7.5, 150 mM NaCl, 1% Triton X-100, 0.1% sodium deoxycholate, 2.5 mM EDTA, 10% glycerol, freshly supplemented with cOmplete™, EDTA-free protease inhibitor cocktail (Cat# 04693132001) and 1 mM PMSF (Sigma). After brief incubation of 15 minutes, sample solutions were filtered using Falcon® 40 µm cell strainer (Cat# 352340). Filtrate was centrifuged at 4°C to pellet the nuclei. The pellet was resuspended in an ice-cold nuclei lysis buffer (50 mM Tris-HCl, pH 8; 5 mM EDTA, pH 8; 0.5% SDS). The solution was sonicated for 8 cycles of 10 seconds with 20 seconds gap at 39% amplitude (Branson Sonifier, Marshall Scientific). 1.1% triton was added to the sonicated sample and centrifuged to isolate the supernatant. Preclearing of the sample was done by adding 20 µl of Dynabeads™ Protein G (Invitrogen, Cat# 10003D) and incubated at 4 ℃ for 2h. An aliquot of the sample was stored as Input for the experiment. The sample was incubated with mouse monoclonal antibody to H3K27me3 (Cat# ab6002; Abcam) overnight at 4℃, and Dynabeads™ Protein G was added to immunoprecipitate the DNA fragment for 5 hr at 4℃. Sequential washes were performed in the beads using cold low salt wash buffer (150 mM NaCl, 0.2% SDS, 0.5% Triton X-100, 2 mM EDTA pH 8, 20 mM Tris-HCl pH 8), cold high salt wash buffer (500 mM NaCl, 0.2% SDS, 0.5% Triton X-100, 2 mM EDTA pH 8, 20 mM Tris-HCl pH 8), cold 250mM LiCl wash buffer (0.25 M LiCl, 0.5% NP-40, 0.5% sodium deoxycholate, 1 mM EDTA pH 8, 10 mM Tris-HCl pH 8) and 0.5X TE. All washes were done twice. Magnetic beads were collected and resuspended in TES (25 mM Tris-HCl pH 8, 5 mM EDTA pH 8, 0.5% SDS). 5 M NaCl was added to the sample and input control to reverse the cross-links overnight at 65℃. DNA fragments were purified using a PCR purification kit (Cat #28106, Qiagen). Library constructions were performed, and validated using Qubit and Agilent TapeStation, followed by 150bp

paired-end sequencing on Illumina NovaSeq 6000 by miBiome Therapeutics LLP, Mumbai, India.

The trimmed reads were aligned to reference genome TAIR10, using BWA 0.7.17-r1188 (Li 2013). The quality check of the alignments was done using Qualimap 2.2.2-dev (Okonechnikov *et al.* 2016). Duplicated reads, reads with low mapping quality, and mitochondrial and plastid reads were identified and removed with Samtools version 1.2 (Li *et al.* 2009). Enriched intervals between the IP sample and its relative Input were identified by MACS2 (version 2.0.10) program (Zhang *et al.* 2008) with the default setting. The big-Wig files were generated from the BAM files using Deeptools 3.5.1 (Ramírez *et al.* 2016). The coverage is calculated as the number of reads per bin and normalized to 1 x sequencing depth (reads per genome coverage, RPGC). The resulting bigWig files were visualized in Integrated Genome Viewer (https://igv.org/app/) (Robinson *et al.* 2011) to observe the protein binding on the chromatin. Peak annotation and GO and KEGG analysis for the target regions were done using ChIPseeker 1.32.1 (Yu *et al.* 2015) and ClusterProfiler 4.4.4 (Yu *et al.* 2012).

Whole genome Bisulfite sequencing

To identify changes in DNA methylation, we performed bisulfite sequencing as described previously (Bondada *et al.* 2020). For this, we isolated genomic DNA from 500 mg of micro dissected shoot apices, devoid of cotyledons and hypocotyl, from 2 to 3-day-old WT and *mea*-1$^{-/-}$;*dme*-2$^{-/-}$ seedlings using NucleoSpin® Plant II (MACHEREY-NAGEL). 200 ng of DNA was subjected to fragmentation using ultrasonicator (Covaris) to get an average insert size of 250- 300 bp. The fragments were end repaired, ligated to Enzymatic Methyl (EM)-seq adapters and excess adapter removed using AMPure XP purification beads. This was followed by two sets of enzymatic conversion steps using the Enzymatic Methyl-seq kit (NEB, Cat# E7120L) to differentiate cytosines from 5mC and 5hmC. The resulting converted sequences of the bisulfite-treated adapter ligated library were PCR enriched and clean-up of library products performed as instructed by the manufacturer. The cleaned libraries were quantitated on Qubit fluorometer and appropriate dilutions loaded on a HSD1000 screen tape to determine the size range of the fragments and the average library size.

Prepared library was 150bp paired-end sequenced on Illumina NovaSeq 6000 by miBiome Therapeutics LLP, Mumbai, India. Trimgalore 0.6.7 was used for the Illumina adapter removal. Each sample contained more than 40 million reads. FASTQC v0.11.9 was used for Illumina reads quality check. We used Bismark software utilizing Bowtie2 to align the clean reads to the TAIR10 reference genome, and more than 79% of the reads were uniquely mapped to the *Arabidopsis* genome in each sample (Supplementary Figure 6). Bismark v0.24.0 was used to map the Illumina reads to the reference genome from TAIR10 (Krueger and Andrews 2011). Deduplication, extraction of methylation calls was also performed using Bismark v0.24.0. After removing duplicated reads, the number of methylated and unmethylated reads along with their trinucleotide context was generated for each cytosine on both the strands. The cytosines with overall coverage equal or more than five were considered for methylation calling. The cytosine with five or above-methylated reads or more than 40% of the reads were considered as methylated. Statistical analysis was performed using MethylKit 1.22.0 (Akalin *et al.* 2012). The differential methylation events were annotated for gene features using the ChIPseeker package (Yu *et al.* 2015).

Microscopy and imaging

Bright-field images of seedlings were captured using Leica M205FA stereo microscope. Confocal laser scanning microscopic images were acquired using Zeiss LSM 880 and Leica TCS SP5 II confocal laser-scanning microscope. The confocal imaging was carried out on dissected embryos and 3 to 5 dpg old seedlings using Argon laser source at 40% power. The excitation wavelengths were as follows: 488 nm- for GFP and 514 nm- for YFP. Auto-fluorescence was captured at the wavelength of 633 nm. Images were captured with 40x (oil) or 63x (oil) objectives with 550-750 master gain, 100-200 range pinhole, and frame size of 1,024 by 1,024 pixels. Master gain and the pinhole adjustment varied with samples. The line averaging was adjusted to four and the digital zoom to 0.6. Z-stack images were taken in 5 µm or 1 µm intervals. The whole plant images are captured using a Canon 70D SLR camera. The images are edited in Adobe Photoshop CS4.

Plasmid construction, molecular cloning, and plant transformation

For cloning the gene and its regulatory sequences, the sequence of interest was PCR amplified from total genomic DNA isolated by CTAB method. For cDNA cloning, total RNA was isolated using TRIzol™ reagent as per the manufacturer's instructions. One microgram of DNase-free RNA was used for cDNA synthesis by PrimeScript 1st strand cDNA synthesis kit using an oligo(dT) and random hexamer as oligonucleotides . Polymerase chain reaction (PCR) was carried out using PrimeSTAR® GXL DNA Polymerase (TAKARA-Bio, Cat# R050). The PCR conditions were specific to each sequence and amplified using 10 µM sequence-specific paired oligonucleotides (see Supplementary Table 5) using Applied Biosystems™ ProFlex™ 3 x 32-well PCR System. All entry clones were propagated in DH5α strain of *E.coli* using a single Gateway cloning system. To knock down the expression of *STM*, 272 bp exon sequence was amplified from *cDNA* using region-specific oligonucleotides and cloned in the p2R3E-As-OScT vector (sense) and p221Z-S-Intr vector (antisense) using *Bam*HI and *Xho*I restriction digestion and ligation. All entry clones were propagated in the DH5α strain of E.coli using a single gateway cloning system. The sense and antisense for STM were cloned under *pG1090* inducible promoter (Zuo *et al.* 2000) and subsequently in *pCAMBIA-based R4R3* destination vector. Similarly, the *PLT5* (299 bp) and *CUC2* (Varapparambath *et al.* 2022) knockdown constructs were cloned under *pG1090* inducible promoter to silence the transcript level of *PLT5* and *CUC2*, respectively. To generate *pDME*::*3X-VENUS*:*3AT*, 5000bp upstream regulatory sequence of *DME* is tagged with *3X-VENUS* and *3AT* terminator. Similarly, 5142bp of *MEA* promoter was tagged with *3X-VENUS* to generate *pMEA*::*3X-VENUS*:*3AT*. Translation fusion lines of DME (*pDME*::*gDME*:*vYFP*) and MEA (*pMEA*::*gMEA*:*vYFP*) were generated using three fragments multisite recombination gateway cloning system where the above-mentioned upstream regulatory sequences of *DME* and *MEA* were cloned to drive *DME* (8303 bp) and *MEA* (4199 bp) genomic sequences fused with *vYFP*.

Estradiol treatment for inducible gene knock-down

Inducible RNAi for *STM*, *PLT5*, and *CUC2* genes was carried out, as mentioned earlier (Varapparambath *et al.* 2022). MS agar medium supplemented with 5µM β-estradiol was used to induce conditional gene silencing using *pG1090*:*XVE* artificial

promoter throughout seed germination. Estradiol-treated and mock (DMSO) treated seedlings were scored for ectopic shoot emergence at 15 dpg.

Statistical analysis

The details of the statistical analysis followed in this study are described in the respective figure legends (number of samples (n), mean± S.E.M). The statistical significance levels were defined as $*p < 0.05$, $**p < 0.01$, $***p < 0.001$, $****p < 0.0001$. For mRNA quantitative analysis, statistical significance was determined using the Multiple unpaired *t*-tests (Holm-Sidak method), with alpha = 0.05. For RNAi phenotype quantitative analysis, statistical significance was determined using two-way ANOVA (Sidak method), with alpha = 0.05. All the statistical tests and analyses were performed using GraphPad PRISM (v9.5.1) statistical software.

Data Availability

The ChIP-sequencing and whole-genome bisulfite sequencing data generated and analyzed during the current study are available from NCBI under the bio project accession PRJNA972183 consisting of eight SRA accession identifiers: SRR24547737**,** SRR24547736**,** SRR24547733, SRR24547734, SRR24547735, SRR24547732, SRR25392706 and SRR25392707. All other source data are included in the article as Supplementary Table 2 and 3.

Acknowledgments

M.P.R. thanks to the IISER Thiruvananthapuram for providing a Ph.D. research fellowship. S.S. is a recipient of the Department of Science and Technology (DST) - INSPIRE scholarship for higher education (SHE). R.B. is the recipient of a Junior and Senior Research Fellowship (J.R.F. and S.R.F.) for a Ph.D. funded by the University Grants Commission (U.G.C.), Govt. of India. A.P.S. thanks to the Council of Scientific and Industrial Research (CSIR) for the Ph.D. fellowship. K.P. acknowledges grants from the Department of Biotechnology (D.B.T.), Government of India (BT/PR41931/BRB/10/1964/2021), the Science and Engineering Research Board-Scientific and Useful Profound Research Advancement (SERB-SUPRA), Government of India (S.P.R./2021/000109). R.M. acknowledges financial support from Ramalingaswami's re-entry fellowship awarded by the Department of Biotechnology

(D.B.T., Govt. of India) and the Dupont Young Professor grant, Dupont U.S.A. We thank the Indian Institute of Science Education and Research (IISER)- Thiruvananthapuram for intramural financial and infrastructural support.

Author contributions

R.M. conceptualized, designed, and supervised the study. M.P.R. contributed to certain aspects of the study design and carried out most of the experiments. S.S. generated and performed the phenotypic assessment of RNAi lines along M.P.R. R.B. helped generate double mutant lines. A.P.S. performed cloning experiments for producing reporter lines. K.P. designed, supervised, and critically analyzed the study. M.P.R., K.P., and R.M. wrote the manuscript. R.M. and K.P. acquired funds for the study. All the authors read and approved the draft.

Declaration of interests

The authors declare no competing interests.

References

Aichinger E., C. B. R. Villar, R. di Mambro, S. Sabatini, and C. Köhler, 2011 The CHD3 chromatin remodeler PICKLE and polycomb group proteins antagonistically regulate meristem activity in the *Arabidopsis* root. Plant Cell 23: 1047–1060. https://doi.org/10.1105/tpc.111.083352

Aida M., T. Ishida, and M. Tasaka, 1999 Shoot apical meristem and cotyledon formation during *Arabidopsis* embryogenesis: Interaction among the *CUP-SHAPED COTYLEDON* and *SHOOT MERISTEMLESS* genes. Development 126: 1563–1570. https://doi.org/10.1242/dev.126.8.1563

Aida M., T. Vernoux, M. Furutani, J. Traas, and M. Tasaka, 2002 Roles of *PIN-FORMED1* and *MONOPTEROS* in pattern formation of the apical region of the *Arabidopsis* embryo. Development 129: 3965–3974. https://doi.org/10.1242/dev.129.17.3965

Akalin A., M. Kormaksson, S. Li, F. E. Garrett-Bakelman, M. E. Figueroa, *et al.*, 2012 methylKit: a comprehensive R package for the analysis of genome-wide DNA methylation profiles. Genome Biol. 13: R87. https://doi.org/10.1186/gb-2012-13-10-r87

Baubec T., A. Finke, O. Mittelsten Scheid, and A. Pecinka, 2014 Meristem-specific expression of epigenetic regulators safeguards transposon silencing in *Arabidopsis*. EMBO Rep. 15: 446–452. https://doi.org/10.1002/embr.201337915

Bondada R., S. Somasundaram, M. P. Marimuthu, M. A. Badarudeen, V. K. Puthiyaveedu, *et al.*, 2020 Natural epialleles of Arabidopsis *SUPERMAN* display superwoman phenotypes. Commun. Biol. 3: 1–13. https://doi.org/10.1038/s42003-020-01525-9

Borg M., Y. Jacob, D. Susaki, C. LeBlanc, D. Buendía, *et al.*, 2020 Targeted reprogramming of H3K27me3 resets epigenetic memory in plant paternal chromatin. Nat. Cell Biol. 22: 621–629. https://doi.org/10.1038/s41556-020-0515-y

Bouyer D., F. Roudier, M. Heese, E. D. Andersen, D. Gey, *et al.*, 2011 Polycomb repressive complex 2 controls the embryo-to-seedling phase transition. PLoS Genet. 7. https://doi.org/10.1371/journal.pgen.1002014

Bouyer D., A. Kramdi, M. Kassam, M. Heese, A. Schnittger, *et al.*, 2017 DNA methylation dynamics during early plant life. Genome Biol. 18: 1–12. https://doi.org/10.1186/s13059-017-1313-0

Calarco J. P., F. Borges, M. T. A. Donoghue, F. Van Ex, P. E. Jullien, *et al.*, 2012 Reprogramming of DNA methylation in pollen guides epigenetic inheritance via small RNA. Cell 151: 194–205. https://doi.org/10.1016/j.cell.2012.09.001

Chen D., A. Molitor, C. Liu, and W. H. Shen, 2010 The *arabidopsis* PRC1-like ring-finger proteins are necessary for repression of embryonic traits during vegetative growth. Cell Res. 20: 1332–1344. https://doi.org/10.1038/cr.2010.151

Chen D., A. M. Molitor, L. Xu, and W.-H. Shen, 2016 *Arabidopsis* PRC1 core component AtRING1 regulates stem cell-determining carpel development mainly through repression of class I KNOX genes. BMC Biol. 14: 112. https://doi.org/10.1186/s12915-016-0336-4

Choi Y., M. Gehring, L. Johnson, M. Hannon, J. J. Harada, *et al.*, 2002 *DEMETER*, a DNA glycosylase domain protein, is required for endosperm gene imprinting and seed viability in *Arabidopsis*. Cell 110: 33–42. https://doi.org/10.1016/S0092-8674(02)00807-3

Cui X., F. Lu, Q. Qiu, B. Zhou, L. Gu, *et al.*, 2016 REF6 recognizes a specific DNA sequence to demethylate H3K27me3 and regulate organ boundary formation in *Arabidopsis*. Nat. Genet. 48: 694–699. https://doi.org/10.1038/ng.3556

Daimon Y., K. Takabe, and M. Tasaka, 2003 The *CUP-SHAPED COTYLEDON* Genes Promote Adventitious Shoot Formation on Calli. Plant Cell Physiol. 44: 113–121. https://doi.org/10.1093/pcp/pcg038

Dasgupta P., and S. Chaudhuri, 2019 Analysis of DNA methylation profile in plants by chop-PCR, pp. 79–90 in *Methods in Molecular Biology*,.

De Lucia F., P. Crevillen, A. M. E. Jones, T. Greb, and C. Dean, 2008 A PHD-polycomb repressive complex 2 triggers the epigenetic silencing of FLC during vernalization. Proc. Natl. Acad. Sci. U. S. A. 105: 16831–16836. https://doi.org/10.1073/pnas.0808687105

Du J., L. M. Johnson, S. E. Jacobsen, and D. J. Patel, 2015 DNA methylation pathways and their crosstalk with histone methylation. Nat. Rev. Mol. Cell Biol. 16: 519–532. https://doi.org/10.1038/nrm4043

Feng S., S. E. Jacobsen, and W. Reik, 2010 Epigenetic Reprogramming in Plant and Animal Development. Science 330: 622–627. https://doi.org/10.1126/science.1190614

Figueiredo D. D., R. A. Batista, P. J. Roszak, and C. Köhler, 2015 Auxin production couples endosperm development to fertilization. Nat. Plants 1: 1–6. https://doi.org/10.1038/nplants.2015.184

Gehring M., J. H. Huh, T.-F. F. Hsieh, J. Penterman, Y. Choi, *et al.*, 2006 *DEMETER* DNA Glycosylase Establishes *MEDEA* Polycomb Gene Self-Imprinting by Allele-Specific Demethylation. Cell 124: 495–506. https://doi.org/10.1016/j.cell.2005.12.034.

Grossniklaus U., J. P. Vielle-Calzada, M. A. Hoeppner, and W. B. Gagliano, 1998 Maternal control of embryogenesis by *MEDEA*, a Polycomb group gene in *Arabidopsis*. Science 280: 446–450. https://doi.org/10.1126/science.280.5362.446

Guitton A.-E., D. R. Page, P. Chambrier, C. Lionnet, J.-E. Faure, *et al.*, 2004 Identification of new members of Fertilisation Independent Seed Polycomb Group pathway involved in the control of seed development in *Arabidopsis thaliana*. Development 131: 2971–81. https://doi.org/10.1242/dev.01168

Gutzat R., L. Borghi, J. Fütterer, S. Bischof, Y. Laizet, *et al.*, 2011 RETINOBLASTOMA-RELATED PROTEIN controls the transition to autotrophic plant development. Development 138: 2977–86. https://doi.org/10.1242/dev.060830

Gutzat R., K. Rembart, T. Nussbaumer, F. Hofmann, R. Pisupati, *et al.*, 2020 *Arabidopsis* shoot stem cells display dynamic transcription and DNA methylation patterns. EMBO J. 39: e103667. https://doi.org/10.15252/embj.2019103667

Heisler M. G., C. Ohno, P. Das, P. Sieber, G. V. Reddy, *et al.*, 2005 Patterns of auxin transport and gene expression during primordium development revealed by live imaging of the *Arabidopsis* inflorescence meristem. Curr. Biol. 15: 1899–1911. https://doi.org/10.1016/j.cub.2005.09.052

Higo A., N. Saihara, F. Miura, Y. Higashi, M. Yamada, *et al.*, 2020 DNA methylation is reconfigured at the onset of reproduction in rice shoot apical meristem. Nat. Commun. 11: 1–12. https://doi.org/10.1038/s41467-020-17963-2

Hofhuis H., M. Laskowski, Y. Du, K. Prasad, S. Grigg, *et al.*, 2013 Phyllotaxis and rhizotaxis in *Arabidopsis* are modified by three plethora transcription factors. Curr. Biol. 23: 956–962. https://doi.org/10.1016/j.cub.2013.04.048

Ibarra C. A., X. Feng, V. K. Schoft, T. F. Hsieh, R. Uzawa, *et al.*, 2012 Active DNA demethylation in plant companion cells reinforces transposon methylation in gametes. Science 337: 1360–1364. https://doi.org/10.1126/science.1224839

Iwasaki M., and J. Paszkowski, 2014 Epigenetic memory in plants. EMBO J. 33: 1987–1998. https://doi.org/10.15252/embj.201488883

Jullien P. E., D. Susaki, R. Yelagandula, T. Higashiyama, and F. Berger, 2012 DNA Methylation Dynamics during Sexual Reproduction in *Arabidopsis thaliana*. Curr. Biol. 22: 1825–1830. https://doi.org/10.1016/j.cub.2012.07.061

Kareem A., K. Durgaprasad, K. Sugimoto, Y. Du, A. J. Pulianmackal, *et al.*, 2015 *PLETHORA* genes control regeneration by a two-step mechanism. Curr. Biol. 25: 1017–1030. https://doi.org/10.1016/j.cub.2015.02.022

Khouider S., F. Borges, C. LeBlanc, A. Ungru, A. Schnittger, *et al.*, 2021 Male fertility in *Arabidopsis* requires active DNA demethylation of genes that control pollen tube function. Nat. Commun. 12: 1–10. https://doi.org/10.1038/s41467-020-20606-1

Kim M., H. Ohr, J. W. Lee, Y. Hyun, R. L. Fischer, *et al.*, 2008 Temporal and Spatial Downregulation of *Arabidopsis* MET1 Activity Results in Global DNA Hypomethylation and Developmental Defects. Mol. Cells 26: 611–615.

Kim S., J.-S. S. Park, J. Lee, K. K. Lee, O.-S. S. Park, *et al.*, 2021 The *DME* demethylase regulates sporophyte gene expression, cell proliferation, differentiation, and meristem resurrection. Proc. Natl. Acad. Sci. U. S. A. 118. https://doi.org/10.1073/pnas.2026806118

Köhler C., L. Hennig, C. Spillane, S. Pien, and W. Gruissem, 2003 The Polycomb-group protein *MEDEA* regulates seed development by controlling expression of the MADS-box gene *PHERES1*. Genes Dev. 17: 1540–1553. https://doi.org/10.1101/gad.257403.431

Krueger F., and S. R. Andrews, 2011 Bismark: a flexible aligner and methylation caller for Bisulfite-Seq applications. Bioinformatics 27: 1571–1572. https://doi.org/10.1093/bioinformatics/btr167

Kwon C. S., K. I. Hibara, J. Pfluger, S. Bezhani, H. Metha, *et al.*, 2006 A role for chromatin remodeling in regulation of *CUC* gene expression in the *Arabidopsis* cotyledon boundary. Development 133: 3223–3230. https://doi.org/10.1242/dev.02508

Lafos M., P. Kroll, M. L. Hohenstatt, F. L. Thorpe, O. Clarenz, *et al.*, 2011 Dynamic Regulation of H3K27 Trimethylation during *Arabidopsis* Differentiation. PLOS Genet. 7: e1002040. https://doi.org/10.1371/journal.pgen.1002040

Lee K., and P. J. Seo, 2018 Dynamic Epigenetic Changes during Plant Regeneration. Trends Plant Sci. 23: 235–247. https://doi.org/10.1016/j.tplants.2017.11.009

Li H., B. Handsaker, A. Wysoker, T. Fennell, J. Ruan, *et al.*, 2009 The Sequence Alignment/Map format and SAMtools. Bioinformatics 25: 2078–2079. https://doi.org/10.1093/bioinformatics/btp352

Li Z. H., X. Lu, Y. Gao, S. J. Liu, M. Tao, *et al.*, 2011 Polyploidization and epigenetics. Chin. Sci. Bull. 56: 245–252. https://doi.org/10.1007/s11434-010-4290-1

Li H., 2013 Aligning sequence reads, clone sequences and assembly contigs with BWA-MEM. ArXiv Prepr. 1303: 3997.

Lindsey B. E., L. Rivero, C. S. Calhoun, E. Grotewold, and J. Brkljacic, 2017 Standardized method for high-throughput sterilization of *Arabidopsis* seeds. J. Vis. Exp. 2017: 1–7. https://doi.org/10.3791/56587

Livak K. J., and T. D. Schmittgen, 2001 Analysis of Relative Gene Expression Data Using Real-Time Quantitative PCR and the 2−ΔΔCT Method. Methods 25: 402–408. https://doi.org/10.1006/meth.2001.1262

Lodha M., C. F. Marco, and M. C. P. Timmermans, 2013 The ASYMMETRIC LEAVES complex maintains repression of KNOX homeobox genes via direct recruitment of Polycomb-repressive complex2. Genes Dev. 27: 596–601. https://doi.org/10.1101/gad.211425.112

Luo M., P. Bilodeau, E. S. Dennis, W. J. Peacock, and a Chaudhury, 2000 Expression and parent-of-origin effects for FIS2, MEA, and FIE in the endosperm and embryo of developing *Arabidopsis* seeds. Proc. Natl. Acad. Sci. U. S. A. 97: 10637–10642. https://doi.org/10.1073/pnas.170292997

Mayer K. F. X., H. Schoof, A. Haecker, M. Lenhard, G. Jurgens, *et al.*, 1998 Role of WUSCHEL in Regulating Stem Cell Fate in the *Arabidopsis* Shoot Meristem. Cell 95: 805–815. https://doi.org/10.1111/j.1365-2818.1977.tb01111.x

Moreno-Romero J., H. Jiang, J. Santos-González, and C. Köhler, 2016 Parental epigenetic asymmetry of PRC 2-mediated histone modifications in the *Arabidopsis* endosperm. EMBO J. 35: 1298–1311. https://doi.org/10.15252/embj.201593534

Okonechnikov K., A. Conesa, and F. García-Alcalde, 2016 Qualimap 2: Advanced multi-sample quality control for high-throughput sequencing data. Bioinformatics 32: 292–294. https://doi.org/10.1093/bioinformatics/btv566

Park J. S., J. M. Frost, K. Park, H. Ohr, G. T. Park, *et al.*, 2017 Control of *DEMETER* DNA demethylase gene transcription in male and female gamete companion cells in *Arabidopsis thaliana*. Proc. Natl. Acad. Sci. U. S. A. 114: 2078–2083. https://doi.org/10.1073/pnas.1620592114

Park K., S. Lee, H. Yoo, and Y. Choi, 2020 DEMETER-mediated DNA Demethylation in Gamete Companion Cells and the Endosperm, and its Possible Role in Embryo Development in *Arabidopsis*. J. Plant Biol. 63: 321–329. https://doi.org/10.1007/s12374-020-09258-2

Pires N. D., M. Bemer, L. M. Müller, C. Baroux, C. Spillane, *et al.*, 2016 Quantitative Genetics Identifies Cryptic Genetic Variation Involved in the Paternal Regulation of Seed Development, (G. Gibson, Ed.). PLOS Genet. 12: e1005806. https://doi.org/10.1371/journal.pgen.1005806

Prasad K., S. P. Grigg, M. Barkoulas, R. K. Yadav, G. F. Sanchez-Perez, *et al.*, 2011 *Arabidopsis* PLETHORA transcription factors control phyllotaxis. Curr. Biol. 21: 1123–1128. https://doi.org/10.1016/j.cub.2011.05.009

Qiu Q., H. Mei, X. Deng, K. He, B. Wu, *et al.*, 2019 DNA methylation repels targeting of *Arabidopsis* REF6. Nat. Commun. 10: 1–9. https://doi.org/10.1038/s41467-019-10026-1

Ramírez F., D. P. Ryan, B. Grüning, V. Bhardwaj, F. Kilpert, *et al.*, 2016 deepTools2: a next generation web server for deep-sequencing data analysis. Nucleic Acids Res. 44: W160–W165. https://doi.org/10.1093/NAR/GKW257

Ravi M., and S. W. L. Chan, 2010 Haploid plants produced by centromere-mediated genome elimination. Nature 464: 615–618. https://doi.org/10.1038/nature08842

Ravi M., M. P. A. Marimuthu, E. H. Tan, S. Maheshwari, I. M. Henry, *et al.*, 2014 A haploid genetics toolbox for *Arabidopsis thaliana*. Nat. Commun. 5: 1–8. https://doi.org/10.1038/ncomms6334

Ravi M., and R. Bondada, 2016 Genome Elimination by *tailswap* CENH3: In Vivo Haploid Production in *Arabidopsis*. Methods Mol. Biol. 1469,77–99 (2016)

Robinson J. T., H. Thorvaldsdóttir, W. Winckler, M. Guttman, E. S. Lander, *et al.*, 2011 Integrative genomics viewer. Nat. Biotechnol. 29: 24–26. https://doi.org/10.1038/nbt.1754

Roszak P. J., and C. Köhler, 2011 Polycomb group proteins are required to couple seed coat initiation to fertilization. Proc. Natl. Acad. Sci. U. S. A. 108: 20826–20831. https://doi.org/10.1073/pnas.1117111108

Roy S., P. Gupta, M. P. Rajabhoj, R. Maruthachalam, and A. K. Nandi, 2018 The polycomb-group repressor MEDEA attenuates pathogen defense. Plant Physiol. 177: 1728–1742. https://doi.org/10.1104/pp.17.01579

Salvi E., J. P. Rutten, R. Di Mambro, L. Polverari, V. Licursi, *et al.*, 2020 A Self-Organized PLT/Auxin/ARR-B Network Controls the Dynamics of Root Zonation Development in *Arabidopsis thaliana*. Dev. Cell 53: 431-443.e23. https://doi.org/10.1016/j.devcel.2020.04.004

Schmid M., T. S. Davison, S. R. Henz, U. J. Pape, M. Demar, *et al.*, 2005 A gene expression map of *Arabidopsis thaliana* development. Nat. Genet. 37: 501–506. https://doi.org/10.1038/ng1543

Schoft V. K., N. Chumak, Y. Choi, M. Hannon, M. Garcia-Aguilar, *et al.*, 2011 Function of the DEMETER DNA glycosylase in the *Arabidopsis thaliana* male gametophyte. Proc Natl Acad Sci USA 108: 8042–7. https://doi.org/10.1073/pnas.1105117108

Schoof H., M. Lenhard, A. Haecker, K. F. X. Mayer, G. Jürgens, *et al.*, 2000 The stem cell population of *Arabidopsis* shoot meristems is maintained by a regulato-

ry loop between the *CLAVATA* and *WUSCHEL* genes. Cell 100: 635–644. https://doi.org/10.1016/S0092-8674(00)80700-X

Schumann U., J. M. Lee, N. A. Smith, C. Zhong, J. K. Zhu, *et al.*, 2019 DEMETER plays a role in DNA demethylation and disease response in somatic tissues of *Arabidopsis*. Epigenetics 14: 1074–1087. https://doi.org/10.1080/15592294.2019.1631113

Scofield S., W. Dewitte, and J. A. Murray, 2008 A model for *Arabidopsis* class-1 KNOX gene function. Plant Signal. Behav. 3: 257–259. https://doi.org/10.4161/psb.3.4.5194

Shen W.-H., and L. Xu, 2009 Chromatin Remodeling in Stem Cell Maintenance in *Arabidopsis thaliana*. Mol. Plant 2: 600–609. https://doi.org/10.1093/mp/ssp022

Simonini S., M. Bemer, S. Bencivenga, V. Gagliardini, N. D. Pires, *et al.*, 2021 The Polycomb group protein MEDEA controls cell proliferation and embryonic patterning in *Arabidopsis*. Dev. Cell 56: 1945-1960.e7. https://doi.org/10.1016/j.devcel.2021.06.004

Slotkin R. K., M. Vaughn, F. Borges, M. Tanurdžić, J. D. Becker, *et al.*, 2009 Epigenetic Reprogramming and Small RNA Silencing of Transposable Elements in Pollen. Cell 136: 461–472. https://doi.org/10.1016/j.cell.2008.12.038

Spillane C., K. J. Schmid, S. Laoueillé-Duprat, S. Pien, J.-M. Escobar-Restrepo, *et al.*, 2007 Positive darwinian selection at the imprinted *MEDEA* locus in plants. Nature 448: 349–352. https://doi.org/10.1038/nature05984

Spinelli S. V., A. P. Martin, I. L. Viola, D. H. Gonzalez, and J. F. Palatnik, 2011 A Mechanistic Link between *STM* and *CUC1* during *Arabidopsis* Development. Plant Physiol. 156: 1894–1904. https://doi.org/10.1104/pp.111.177709

Stahl Y., and R. Simon, 2010 Plant primary meristems: shared functions and regulatory mechanisms. Curr. Opin. Plant Biol. 13: 53–58. https://doi.org/10.1016/j.pbi.2009.09.008

Sun B., L. S. Looi, S. Guo, Z. He, E. S. Gan, *et al.*, 2014 Timing mechanism dependent on cell division is invoked by Polycomb eviction in plant stem cells. Science 343. https://doi.org/10.1126/science.1248559

Ten Hove C. A., K. J. Lu, and D. Weijers, 2015 Building a plant: Cell fate specification in the early *Arabidopsis* embryo. Dev. Camb. 142: 420–430. https://doi.org/10.1242/dev.111500

Varapparambath V., M. M. Mathew, A. P. Shanmukhan, D. Radhakrishnan, A. Kareem, *et al.*, 2022 Mechanical conflict caused by a cell-wall-loosening enzyme activates de novo shoot regeneration. Dev. Cell 57: 2063–2080. https://doi.org/10.1016/j.devcel.2022.07.017

Vielle-Calzada J. P., J. Thomas, C. Spillane, A. Coluccio, M. A. Hoeppner, *et al.*, 1999 Maintenance of genomic imprinting at the *Arabidopsis* medea locus re-

quires zygotic DDM1 activity. Genes Dev. 13: 2971–2982. https://doi.org/10.1101/gad.13.22.2971

Williams B. P., and M. Gehring, 2020 Principles of Epigenetic Homeostasis Shared Between Flowering Plants and Mammals. Trends Genet. 36: 751–763. https://doi.org/10.1016/j.tig.2020.06.019

Williams B. P., L. L. Bechen, D. A. Pohlmann, and M. Gehring, 2022 Somatic DNA demethylation generates tissue-specific methylation states and impacts flowering time. Plant Cell 34: 1189–1206. https://doi.org/10.1093/plcell/koab319

Xiao W., M. Gehring, Y. Choi, L. Margossian, H. Pu, *et al.*, 2003 Imprinting of the *MEA* polycomb gene is controlled by antagonism between MET1 methyltransferase and DME glycosylase. Dev. Cell 5: 891–901. https://doi.org/10.1016/S1534-5807(03)00361-7

Xiao J., and D. Wagner, 2015 Polycomb repression in the regulation of growth and development in *Arabidopsis*. Curr. Opin. Plant Biol. 23: 15–24. https://doi.org/10.1016/j.pbi.2014.10.003

Xiao J., U.-S. Lee, and D. Wagner, 2016 Tug of war: adding and removing histone lysine methylation in *Arabidopsis*. Curr. Opin. Plant Biol. 34: 41–53. https://doi.org/10.1016/j.pbi.2016.08.002

Xiao J., R. Jin, X. Yu, M. Shen, J. D. Wagner, *et al.*, 2017 Cis and trans determinants of epigenetic silencing by Polycomb repressive complex 2 in *Arabidopsis*. Nat. Genet. 49: 1546–1552. https://doi.org/10.1038/ng.3937

Xu L., and W. H. Shen, 2008 Polycomb Silencing of KNOX Genes Confines Shoot Stem Cell Niches in *Arabidopsis*. Curr. Biol. 18: 1966–1971. https://doi.org/10.1016/j.cub.2008.11.019

Yamaguchi N., C. M. Winter, M.-F. Wu, C. S. Kwon, D. A. William, *et al.*, 2014 PROTOCOL: Chromatin Immunoprecipitation from *Arabidopsis* Tissues, p. e0170 in *The Arabidopsis Book*,.

Yoshida N., Y. Yanai, L. Chen, Y. Kato, J. Hiratsuka, *et al.*, 2001 EMBRYONIC FLOWER2, a novel Polycomb group protein homolog, mediates shoot development and flowering in *Arabidopsis*. Plant Cell 13: 2471–2481. https://doi.org/10.1105/tpc.13.11.2471

You Y., A. Sawikowska, M. Neumann, D. Posé, G. Capovilla, *et al.*, 2017 Temporal dynamics of gene expression and histone marks at the *Arabidopsis* shoot meristem during flowering. Nat. Commun. 8: 15120. https://doi.org/10.1038/ncomms15120

Yu G., L. G. Wang, Y. Han, and Q. Y. He, 2012 ClusterProfiler: An R package for comparing biological themes among gene clusters. OMICS J. Integr. Biol. 16: 284–287. https://doi.org/10.1089/omi.2011.0118

Yu G., L. G. Wang, and Q. Y. He, 2015 ChIP seeker: An R/Bioconductor package for ChIP peak annotation, comparison and visualization. Bioinformatics 31: 2382–2383. https://doi.org/10.1093/bioinformatics/btv145

Zhang X., O. Clarenz, S. Cokus, Y. V. Bernatavichute, M. Pellegrini, *et al.*, 2007 Whole-Genome Analysis of Histone H3 Lysine 27 Trimethylation in *Arabidopsis*, (J. C. Carrington, Ed.). PLoS Biol. 5: e129. https://doi.org/10.1371/journal.pbio.0050129

Zhang Y., T. Liu, C. A. Meyer, J. Eeckhoute, D. S. Johnson, *et al.*, 2008 Model-based Analysis of ChIP-Seq (MACS). Genome Biol. 9: R137. https://doi.org/10.1186/gb-2008-9-9-r137

Zhang H., K. Tang, B. Wang, C. G. Duan, Z. Lang, *et al.*, 2014 Protocol: A beginner's guide to the analysis of RNA-directed DNA methylation in plants. Plant Methods 10: 1–9. https://doi.org/10.1186/1746-4811-10-18

Zhang S., D. Wang, H. Zhang, M. I. Skaggs, A. Lloyd, *et al.*, 2018 FERTILIZATION-INDEPENDENT SEED-Polycomb Repressive Complex 2 Plays a Dual Role in Regulating Type I MADS-Box Genes in Early Endosperm Development. Plant Physiol. 177: 285–299. https://doi.org/10.1104/PP.17.00534

Zuo J., Q. W. Niu, and N. H. Chua, 2000 An estrogen receptor-based transactivator XVE mediates highly inducible gene expression in transgenic plants. Plant J. 24: 265–273. https://doi.org/10.1046/j.1365-313X.2000.00868.x